Computational and Structural Biotechnology Journal 20 (2022) 2042–2056

COMPUTATIONAL AND STRUCTURAL BIOTECHNOLOGY JOURNAL

journal homepage: www.elsevier.com/locate/csbj

SARS-CoV-2 pan-variant inhibitory peptides deter S1-ACE2 interaction and neutralize delta and omicron pseudoviruses

Masaud Shah [a], Sung Ung Moon [a], Jang Hyun Kim [a], Trinh Thanh Thao [a], Hyun Goo Woo [a,b,*]

[a] Department of Physiology, Ajou University School of Medicine, Suwon, Republic of Korea
[b] Department of Biomedical Science, Graduate School, Ajou University, Suwon, Republic of Korea

ARTICLE INFO

Article history:
Received 9 November 2021
Received in revised form 20 April 2022
Accepted 20 April 2022
Available online 26 April 2022

Keywords:
ACE2
Neutralization
Omicron
Peptides-Cocktail
SARS-CoV-2
Spike
VOCs

ABSTRACT

Approved neutralizing antibodies that target the prototype Spike are losing their potency against the emerging variants of concern (VOCs) of SARS-CoV-2, particularly Omicron. Although SARS-CoV-2 is continuously adapting the host environment, emerging variants recognize the same ACE2 receptor for cell entry. Protein and peptide decoys derived from ACE2 or Spike proteins may hold the pan-variant inhibitory potential. Here, we deployed interactive structure- and pharmacophore-based approaches to design short and stable peptides –Coronavirus Spike Neutralizing Peptides (CSNPs)– capable of neutralizing all SARS-CoV-2 VOCs. After *in silico* structural stability investigation and free energies perturbation of the isolated and target-bound peptides, nine candidate peptides were evaluated for the biophysical interaction through SPR assay. CSNP1, CSNP2, and Pep1 dose-dependently bind the S1 domain of the prototype Spike, whereas CSNP4 binds both S1 and ACE2. After safety and immunocytochemistry evaluation, peptides were probed for their pan-variant inhibitory effects. CSNP1, CSNP2, and CSNP4 inhibited all VOCs dose-dependently, whereas Pep1 had a moderate effect. CSNP2 and CSNP4 could neutralize the wild-type pseudovirus up to 80 % when treated at 0.5 μM. Furthermore, CSNP4 synergize the neutralization effect of monoclonal antibody and CSNP1 in Delta variant pseudovirus assay as they target different regions on the RBD. Thus, we suggest that CSNPs are SARS-CoV-2 pan-variant inhibitory candidates for COVID-19 therapy, which may pave the way for combating the emerging immune-escaping variants. We also propose that CSNP1/2-CSNP4 peptide cocktail or CSNP1/4 mAbs cocktail with no overlapping epitopes could be effective therapeutic strategies against COVID-19.

1. Background

SARS-CoV-2 is rapidly evolving, acquiring approximately two mutations per month in the global population [1–2]. As the receptor-binding domain (RBD) in Spike switches between "up" and "down" conformations to facilitate angiotensin-converting enzyme 2 (ACE2) binding and evade immune surveillance [3–4], masking of RBD can lead to the paradox of immune evasion with less infectivity of the virus. Thus, the virus adapted Asp614Gly mutation in Spike, which increased its "up" conformation and the overall density of Spike protein at the virus surface, increasing its infectivity and making it more susceptible to neutralizing antibodies [5–6]. The capacity of host adaptation by SARS-CoV-2 as exemplified by the Asp614Gly mutation [7] and the rise of variants of concern VOCs, including Alpha, Beta, Gamma, Delta, Omicron (BA.1 and BA.2) and other variants of interest including epsilon B.1.427/B.1429, Zeta (P.2), Eta (B1.525), Theta (P.3), Lota (B.1.526), Kappa (B.1.617.1), and Lambda (C.37) [8–9] raised concerns over the efficacy of neutralizing antibodies response that is either induced by the vaccines [9–10], collected from the convalescent plasma or developed in the lab against the wild-type Spike antigen. The Gamma variants have been associated with adverse disease symptoms and even infected a person who has recovered from a previous infection, although this claim needded further definitive data support [11]. The Beta variant was weakly neutralized by the mAbs collected from the convalescent plasma of the patients infected by previous variants [12] and serum obtained from the vaccinees [13]. Preliminary studies based on the data of placebo-controlled vaccine trials suggest that some vaccines are less effective against mild and moderate infections caused by Beta variants [9,14]. Omicron (BA.1), the new variant of concern contains at least 15 mutations in the RBD region [15] and due to the

* Corresponding author at: Department of Physiology, Ajou University School of Medicine, Suwon, Republic of Korea.
E-mail address: hg@ajou.ac.kr (H. Goo Woo).

https://doi.org/10.1016/j.csbj.2022.04.030

triple mutations His655Tyr, Asn679Lys, and Pro681His in the furin cleavage site, this strain is known to be the fastest spreading variant of SARS-CoV-2 [16]. We and others have now confirmed that Omicron escapes most of the FDA-approved antibody-based drugs formulated by Regeneron, AstraZeneca, AbCellera, and other companies [15,17]. Sotrovimab (VIR-7831) and DXP-604, however, retained their Omicron neutralizability at reduced efficacy [17]. Thus, the difficulties in vaccine development and their limitations in the long run against the pandemic due to the continuously evolving nature of Spike suggest the dire need for therapeutic agents that hold pan-variant Spike-ACE2 abrogating abilities.

The knowledge of structural protein–protein interface (PPI) between ACE2 and RBD has been utilized for designing effective therapeutic interventions against SARS-CoV-2 Spike [18–20]. For example, a peptide S471–503, derived from the ACE2 binding region of the SARS-CoV RBD, hinders the ACE2-RBD interaction and viral entry into the cell [21]. Another peptide against SARS-CoV constructed by the glycine linkage of two separate segments (a.a. 22–44 and 351–357) of ACE2 also exhibited efficient antiviral activity [22]. Corroborating this approach, a truncated 23-mer (a.a. 21–43) peptide (SBP1) from the α1 helix of the ACE2 exhibited SARS-CoV-2 glycosylated-RBD-binding in nanomolar concentration (K_D = 47 nM) [23]. However, this binding was only observed in the insect-derived RBD, and the peptides did not show any binding to HEK cell-expressed or other insect-derived SARS-CoV-2-RBD variants.

In this study, we attempted similar but more advanced approaches to design structurally constrained peptides, demonstrating the paradox of spontaneous RBD-conformation switching and the interaction of S1 domain of Spike with soluble and membrane-bound ACE2. Previously, we and others have identified key residues that contribute to the binding strength of ACE2-RBD [3,19–20,24]. Point mutation analyses confirmed that some of these residues are vital to the ACE2-RBD interface [25]. By utilizing this interface knowledge, we identified pharmacophores that are crucial for RBD-ACE2 binding and selected amino acids within the α1 helix of ACE2 that are sub-optimal for the RBD-binding [26]. Exploiting these pharmacophores/hotspots and substituting the suboptimal residues, we designed short Coronavirus Spike Neutralizing Peptides (CSNPs) and evaluated their effect on the S1-hACE2 binding inhibition and the SARS-CoV-2 pseudovirus neutralization in the hACE2-expressing 293 T cells.

2. Methods

2.1. Peptides designing rationale and synthesis

Crystal structure of SARS-CoV-2 Spike-RBD bound to ACE2 (PDB ID: 6M0J) was used to design the helical peptides. For CSNP1-3 and Pep1-5, we identified the hotspot residues in RBD and ACE2 through PDBePISA [27] and evaluated their effects on the interface through alanine scanning by DrugscorePPI [28], which calculate the difference in the binding energy of the wild-type (ΔG^{WT}) and mutant (ΔG^{MUT}) residues at the interface and provide hotspot information. Two regions on the ACE2, a.a. 23–46 and a.a. 352–357 that optimally engage the RBD, were selected to design the parent peptide (CSNP1). Both regions were linked through the GPG loop, and the freedom of Lys353 was restricted by the disulfide bond (S-S) bond, stapling the two beta-sheets at positions Cys350 and Cys356.

An electrostatic surface map was generated around the hotspot and other interface residues using APBS and APBSrun plugins in VMD [29]. Then, the modifiable and vital candidates of pharmacophores in the α1 helix (a.a. 23–46) were identified using the pharmacophore package implemented in MOE (2020.09). Considering the surface complementarity, we identified five potential residues, *i.e.*, Glu23, Lys26, Thr27, His34, and Gln42, for substitution. To enhance the CSNP1-RBD binding, these residues were subsequently substituted by the residues-scan tool in the protein-design package of MOE suit as described previously [30]. Firstly, the mutation window was restricted to one residue only, and the Glycine and self-mutation were excluded during mutant generation. Then, based on binding affinity and stability, the top five mutants were selected and subjected to the second round of residues scan, keeping the mutation window 5. The changes in the binding affinities of the wild-type and mutant peptides were dually evaluated through SSIPe and EvoEF [31]. Structurally constrained peptides have been suggested to retain their structures and grab the shallow surfaces of the targets efficiently [32–34]. To stabilize and maintain the helical structures of the selected peptides, we developed a lactam bridge at the i and i + 4 positions of the non-interface residues, as described in our previous work [35]. For CSNP3, the pharmacophores in the α1 (a.a. 21–46) region of ACE2 were considered, but the a.a. 352–357 regions were excluded. Non-constrained derivatives of the CSNP3, Pep2-5 were also designed. For CSNP4 designing, the trimeric Spike-ACE2 (PDB ID: 6ZXN) and ACE2-RBD complexes were considered as the RBD acquires a different pose in "down" conformation. CSNP4 was designed by linking a.a. 445–456 and a.a. 488–501 motifs of the RBD without implementing the residues scan. CSNP1-4 and Pep1-5 were finally selected as candidate peptides and synthesized by Peptron Inc. (Daejeon, Korea) and Gl-Biochem (China) at a purity of over 95%, as determined by reversed-phase high-performance liquid chromatography (HPLC; Shimadzu Prominence). The HPLC reports and related information about peptide synthesis are provided in supplementary data (see Supplementary methods).

2.2. Molecular dynamics simulation (MDS) analysis of CSNPs

MDS is widely used to study the protein folding and the dynamic behavior of macromolecules in complex or isolated forms. Briefly, default ABMER99-ILDN force-field [36] was used for CSNP1, CSNP4, and SBP1 (a previously identified RBD-binding peptide) simulations, and the same force-field was modified for the lactam bond stapled peptides CSNP2 and CSNP3. New residues and parameters were added into the modified force-field wherever needed. The peptides in their isolated form were simulated for 200 ns and their target-bound complexes for 100 ns. All simulations were carried out in GROMACS 2019.6 in TIP3P water-filled cubic box with 10 Å extended boundaries from the protein. All the systems were neutralized with counter ions, Na^+/Cl^-, wherever needed and energy minimized under steepest descent algorithm, then equilibrated with NVT ensemble for 0.2 ns and re-equilibrated with NPT ensemble for 0.2 ns, under constant temperature and pressure, respectively. The temperature and pressure were coupled with V-rescale and Parrinello-Rahman barostat methods [37], respectively. The bond lengths were constrained with the LINCS algorithm, and long-range electrostatic interactions were computed with the particle mesh Ewald algorithm [38].

2.3. Calculation of the binding free energy by molecular mechanics Poisson–Boltzmann surface area (MMPBSA).

MMPBSA is used for calculating the relative binding energy of ligands bound to the target [39]. We used the g_mmpbsa and APBSA tools implemented in GROMACS for calculating energies. As the g_mmpbsa tool is compatible with older versions of GROMACS (version 5 or earlier), the "tpr" files created by GROMACS 2019.6 were recreated through GROMACS 5.1. The relative binding

energies of the complexes were approximated according to the following energies terms.

$$\Delta G_{bind} = \Delta E_{MM} + \Delta G_{sol}.$$

whereas;

$$\Delta E_{MM} = \Delta E_{cov} + \Delta E_{elec} + \Delta E_{vdW}.$$

and;

$$\Delta G_{sol} = \Delta G_{polar} + \Delta E_{non-polar}.$$

ΔE_{MM} is gas-phase MM-energy change, and ΔG_{sol} is the solvation free energy change. van der Waals energy change (ΔE_{vdW}), the electrostatic energy change (ΔE_{ele}), and the covalent energy change (ΔE_{cov}). The solvation free energy (ΔG_{sol}) is computed by combining both polar and non-polar energies. All these changes were computed via ensemble, which is averaged over a set of conformations sampled over the last 25 ns simulation trajectory at 0.01 ns time interval.

2.4. Computational tools

For visualization and collecting structural insights of the SARS-CoV-2 Spike and ACE2 proteins, free available packages of VMD [29], Pymol (https://pymol.org), and Chimera [40] were utilized. For electrostatic surfaces isolation of the proteins, the APBS and APBSrun plugins in Pymol and VMD, and for monitoring changes in the secondary structures of the peptides as a function of time the sscache.tcl script was used in VMD. 3D animated movies were built using VMD. Interface analysis determining the contribution of each residue into the ACE2-S binding were performed using the online server PDBePISA (v1.52) [27] and the BIOVIA Discovery Studio Visualizer (https://www.accelrys.com). Alanine mutagenesis analysis was performed using the alanine scanning package implemented in the PPCheck hotspot prediction tool [41]. The hotspot results were validated through the DrugScorePPI web server [28,42]. Pharmacophores were evaluated using the ligandScout trial version and MOE [43]. Molecular dynamics was simulated using GROMACS 2019.6 [44]. For MMPBSA calculations, the "tpr" files created by GROMACS 2019.6 were recreated through GROMACS 5.1 and used for binding energies calculations, as described previously [42].

2.5. Surface plasmon resonance (SPR) analysis

For the physical interaction of CSNPs with ACE2 and S1 subunit, SPR assay was conducted using Biacore T200 (GE Healthcare, Sweden). S1 (ligand, AcroBiosystems, S1N-C52H3-100UG, USA) protein was immobilized to the CM5 sensor chip (GE Healthcare, Cat#. BR-1005–30) at 6.0 μg/mL concentration using 10 mM sodium acetate (pH 5.5) as immobilization buffer. ACE2 (Acrobiosystems, ACE2-C52H7-50ug, USA) was immobilized to the same chip at 6.2 μg/mL concentration using a 10 mM sodium acetate immobilization buffer. The following solutions were used as running buffers: 1) HBS (10 mM HEPES, pH 7.4, 150 mM NaCl), 2) HBS-EP (10 mM HEPES, pH 7.4, 150 mM NaCl, 3 mM EDTA, 0.05% P20), 3) HBS with 5% DMSO. NaOH solution (10 ∼ 50) mM was used as a regeneration buffer. The CSNPs and Peps were injected into the ligand-bound chip at different concentrations and their respective k_a, k_d, and K_D values were calculated. The running buffer was injected into the empty channel as a reference. The experiments were conducted in duplicate with freshly prepared reagents, and the data were analyzed in the Software Control (version 2.0.1) and BIAevaluation (version 3.0) software.

2.6. Cells, plasmids, and pseudovirus preparation

The 293T (derived from human embryonic kidney 293 cells that express the large T antigen of simian virus 40) and hACE2-293T cells (293T cells stably overexpressing human ACE2) were cultured in Dulbecco's modified Eagle's medium (DMEM, Gibco, UT, USA) supplemented with 10% fetal bovine serum (FBS, Gibco, NY, USA). 293T cells were purchased from the Korean Cell Line Bank (KCLB, Seoul, Korea) and transfected with pcDNA3.1-hACE2 (Addgene, 145033, USA) plasmids by Lipofectamine 3000 (Invitrogen, L3000015, USA) to produce hACE2 overexpressing hACE2-293T cells. In addition, an HIV dual reporter vector, NL4-3 mCherry Luciferase (Addgene catalog number #44965), expressing mCherry and Luciferase to measure the cells containing reactivated latent provirus simultaneously, and the overall strength of viral transcriptional response was transfected in hACE2-29T cells.

The plasmid HDM-SARS2-Spike-delta21 (Addgene #155130) encoding the SARS-CoV-2 Spike^{WT} lacking 21C-terminal amino acids was used for lentivirus pseudotyping. The plasmid pCDNA3.3_CoV2_B.1.1.7-alpha (Addgene # 170451) that encodes SARS-CoV-2B.1.1.7 (Alpha strain) Spike with an 18aa deletion on the C-terminal tail was used for lentivirus pseudotyping. The plasmid pcDNA3.3_CoV2_501V2-beta (Addgene #170449) encoding SARS-CoV-2 501 V2 (Beta strain) Spike with an 18aa deletion on the C-terminal tail was used for lentivirus pseudotyping. The pcDNA3.3_CoV2_P1-gamma (Addgene #170450) plasmid that encodes SARS-CoV-2P.1 (Gamma) strain Spike with an 18aa deletion on the C-terminal tail was used for lentivirus pseudotyping. The plasmid pcDNA3.3-SARS2-B.1.617.2-delta (Addgene #172320) that encodes SARS-CoV-2B.1.617.2 Spike (delta strain) was used for lentivirus pseudotyping. The plasmid pTwist-SARS-CoV-2 Δ18 B.1.1.529-omicron (Addgene #179907) that encodes SARS-CoV-2B.1.1.529 Spike lacking 18C-terminal amino acids for pseudovirus production.

In addition, the pVSV plasmid that expresses pVSV under a CMV promoter was used to establish the positive control. At 18 to 24 h post-transfection using Lipofectamine 3000 (Invitrogen, L3000015, USA), the culture media was refreshed with pre-warmed growth media. At 60 h post-transfection, Pseudoviruses were harvested by collecting the supernatant from each well and filtering it through a 0.45um filter. Pseudoviruses were stored at 4 °C for immediate use or frozen at −80 °C. Further details about the SARS-CoV-2 Spike pseudovirus generation and propagation have been described previously [45]. The Spike pseudotyped lentiviruses were generated by transfecting 293T cells, seeded in growth media with 50–70% confluence (106 cells per 100 mm dish), with pGag plasmids required for lentiviral production, using Lipofectamine 3000 transfection reagent (Invitrogen, Waltham, MA, USA) at 37 °C in a CO2 incubator. Detailed protocols for SARS-CoV-2 Spike pseudovirus particles production have been described previously [45].

2.7. Immunocytochemistry and confocal microscopy

For CSNPs-binding, hACE2-293T cells were incubated with 10 μM peptide for 1 h and then treated and incubated with 5 μM SARS-CoV-1 S1 protein-His Tag (AcroBiosystems, S1N-C52H3-100UG, USA) for 24 h. The hACE2 over-expression was evaluated in hACE2-293T cells through mRNA expression level using the following primers: (Cosmo Genentech, hACE2-F: 5′-TCC ATT GGT CTT CTG TCA CCC G-3′, hACE2-R: 5′-AGA CCA TCC ACC TCC ACT TCT C-3′, Republic of Korea). After three times whshing with PBS, the cells were incubated with primary antibody anti-ACE2 (1:100, Cell signaling, 4355S, USA), anti-CTNNB1 (1:100, Cell signaling, 8480S, USA), and anti-His-Tag (1:100, Santa Cruz, sc-8036, USA) at 4 °C for 2 h in serum-free media. The cells were fixed with 4%

paraformaldehyde for 5 min and incubated with donkey anti-mouse IgG conjugated with Alexa Fluor 594 (1:200, Thermo, A21203, USA) and donkey anti-rabbit IgG Alexa Fluor 488 (1:200, Thermo, A21206, USA) at room temperature for 2 h. Before the secondary antibodies were incubated, cells were blocked with a blocking solution (1% PBS containing 1% BSA and 0.1% Tween 20) at room temperature for 1 h. All secondary antibodies were diluted in an appropriate concentration of blocking solution. Nuclei were stained with DAPI-containing mounting solution (Vector, H-1200, USA). The cells were then visualized on an LSM710 (Carl Zeiss) confocal microscope.

2.8. Pseudovirus neutralization assay

For the luciferase assay, the hACE2-293T cells were treated with various concentrations (0, 0.01, 0.5, 1, 5, and 10 μM) of peptides and 100 ul of various pseudovirus (Wild, Alpha, Beta, Gamma, Delta, and Omicron) in media. The luciferase activity was measured according to ONE-Glo™ Luciferase Assay System (Promega, USA, E6120) manufacturer's instructions, and a Varioskan Flash Fluorescent Microplate Fluorometer was used without attenuation. For the mCherry fluorescence assay, hACE2-293T cells were treated with pseudovirus in 100ul media and incubated for 48 h. Images were then visualized using an Axiovert 200 fluorescence microscope (Carl Zeiss, Göttingen, Germany). Cell viability was assayed using a Cell Titer-Blue kit (Promega, WI, USA) according to the manufacturer's protocol. For combination effects (synergy) of peptides and antibody (CR3022, cat # ab273073), the Delta pseudovirus neutralization was demonstaretd through luciferase activity. Cells were treated with each drug (CSNP1, CSNP4, and CR3022), in 1uM (peptides) or 500 ng/ml (mAb) concentrations. For synergy, cells were treated drigs in combination of CSNP1 and CSNP4, CSNP1 and CR3022, CSNP4 and CR3022 at suggested concentrations and evaluated further. The concentration of drugs in combination treatment was reduced to half of that used independently.

2.9. Proteinase K assay

Each peptide and bovine serum albumin (BSA) samples were prepared in a base buffer (10 mM Tris-base, 10 mM NaCl, pH 7.4) supplemented with 5 μM $CaCl_2$ and stored as 200 μL of stock solution at a concentration of 50 μM. 30 μL of each sample were removed from the stock for the untreated T0 samples. 5ug/ml ProtK (Bioshop) was then added to a final concentration of the remaining stocks. Samples were incubated at 37 °C, and 30 μL samples were removed at 10, 30, 60 min time point, and the enzymatic activity was immediately blocked by adding 20 mM of PMSF (200 mM stock dissolved in isopropanol). Proteinase K-inactivated samples were frozen at −20 °C until further use. Frozen samples were supplemented with 8 μL of sample loading buffer (4 × NuPAGE; Thermo Fisher Scientific), boiled (50 °C) for 10 min, and centrifuged (13,500RPM, 10 min) before loading onto the gel [12% NuPAGE Bis-Tris (ThermoFisher Scientific)] with 1X Mes running buffer. Gels were run at 200 V for ~35 min and stained using Coomassie Brilliant Blue dye G-250 (Thermo Fisher Scientific). Densitometry of bands was determined using ImageJ software with background subtraction. All samples were normalized by the untreated irrespective sample (T0).

3. Results

3.1. Design of the candidate CSNPs

ACE2 mainly utilizes polar and charged residues in its α1 helix to grab the RBD in its "up" conformation [3] through salt bridges and hydrogen bonds (Table 1). The first three amino acids, Ile21, Glu22, and Glu23 in α1, are exposed to solvent without involving in the RBD binding; nonetheless, these residues are attributable to establishing the α1 helix. Five residues Gln24, Asp30, Lys31, Asp38, and Tyr41 from α1 were the major hotspots that contribute the highest binding energy to the ACE2-RBD complex, as suggested by computational alanine mutagenesis (Fig. S1A, B). In addition to α1 helix, ACE2 utilizes Lys353 to anchor the RBD of both SARS-CoV and SARS-CoV-2 and shares the second-highest binding energy among the ACE2-RBD interface residues (Table 1). Lys353 lies at the hinge of β3-β4 and is stapled by a disulfide bond between Cys344 and Cys361. Therefore, this amino acid might be restricted in its flexibility and freedom, allowing the hydrogen-bond network intact between ACE2 (Lys353) and RBD (Gly496, Gln498, and Gly502) (Fig. 1A). Together, we identified five pharmacophores, *i.e.*, Asp30, Lys31, Asp38, and Tyr41 in α1 and Lys353 in β3-β4, that keep the ACE2-RBD interaction intact (four of them are shown in the electrostatic surface map in Fig. S1C. The $COOH^-$ group of Asp30 serves as a hydrogen bond acceptor in the vicinity of the $NH3^+$ group of Lys417 of RBD. The $NH3^+$ group in the Lys31 of α1 lies between Glu35 of α1 and Glu484 of RBD, establishing a salt bridge between them. The $COOH^-$ group of Asp38 in α1 is indispensable for stabilizing Lys353 in ACE2, making important contacts with Tyr449 and Gln498 of the RBD. The bulky side chains of Tyr41 occupy the hydrophobic space between the a.a. 350–359 segment and the N-terminus of a.a. 21–46 segment in the peptide. Besides, the Tyr41-Thr500 hydrogen bond between ACE2 and RBD restricts the rotation of Tyr41. The $NH3^+$ group of Lys353 is a crucial pharmacophore for the ACE2-RBD interaction (Fig. 1A).

To identify linear and cyclic peptides that block the virus-host cell interaction, a variety of techniques have been utilized, including phage display [46], affinity selection−mass spectrometry [47], cyclic peptide mRNA display [48], and computational tools [49–50]. Short peptides tends to unfold and lose their secondary structures in the solution state upon truncation from tertiary folded proteins. To overcome this issue, researchers have designed peptide biologics by supplementing helical bundles to stabilize the α1 helix and effectively inhibit SARS-CoV-2 cell entry [51–52]. However, this modification increases the size of these peptides by 3–4 fold, increasing the cost of synthesis and formulation. Moreover, bulky peptides may interfere with the neutralizing anti-

Table 1
The Hydrogen bonds at the interface of ACE2-RBD and their bonds-strength in terms of energies.

ACE2	RBD	$E^{kcal/mol}$	Dist Å
Asp30	Lys417	−33.5	2.71
Lys353	G1y496	−11.1	2.71
Lys353	G1n498	−7.3	2.68
Lys31	G1n493	−6.3	2.93
Lys31	G1u484	−5.64	3.24
G1u35	G1n493	−4.9	2.71
Lys353	G1y502	−4.9	2.75
G1u37	Tyr505	−2.8	2.65
G1n24	Asn487	−1.9	2.81
Tyr83	Asn487	−1.7	2.64
G1n42	G1y446	−1.6	2.92
Asp38	G1n498	−1.2	3.57
Lys31	Tyr489	−0.5	4.35

RBD; Receptor binding domain; E, Energy; Dist, distance.

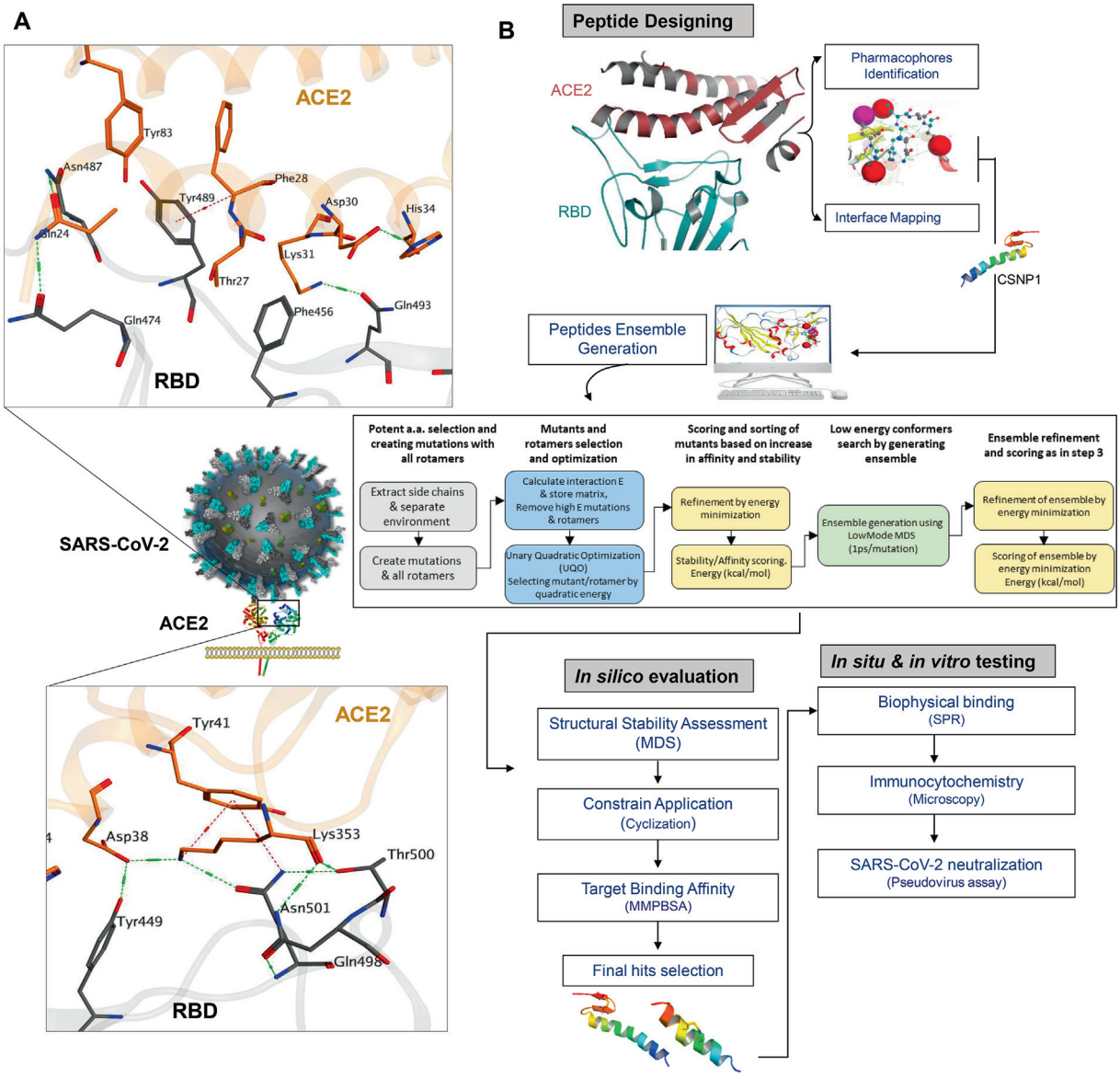

Fig. 1. The SARS-CoV-2 Spike RBD-hACE2 interface analyses and CSNPs peptides designing rationale. A) Identification of the crucial residues at the ACE2-RBD interface using interactive structures and surfaces strategy. B) The overall protocol of CSNPs design. The interface residues and featured pharmacophores were identified and vetted for their energy contribution at the interface. The potential residues were substituted to augment the ACE2-RBD binding. The sequences and secondary structure of the designed CSNPs and SBP1 are shown. Selected peptides were evaluated *in situ* and *in vitro*.

bodies against antigenic Spike. To overcome these limitations, we set up two strategies to design short, stable, and non-bulky peptides that inhibit the receptor interaction and address reversible position-switching of RBD and masking of S1 by soluble ACE2. First, the main scaffold of the α1 helix of ACE2, which is mainly involved in RBD-interaction, was extracted as a starting structure to design and assemble constrained helical CSNPs (CSNP1-3) and linear helical peptides (Pep1-5). Second, the ACE2-interacting motifs of RBD were extracted and assembled into CSNP4 to restrict the RBD movement and block its binding to ACE2.

For the longer helical peptides, the scaffold of α1 helix (a.a. 21–46) of ACE2 was truncated and linked with the β3-β4 (a.a. 350–359) through a Gly-Pro-Gly (GPG) linker. The freedom of Lys353 was restricted by creating an S-S bond between Asp350Cys and Phe356Cys. We designated this peptide as a parent peptide (CSNP1, Fig. 1B). A linear form of the CSNP1, including α1 helix (a.a. 23–46) only, was designated as Pep1 for comparative binding affinity analysis. Next, the complementarity of the electrostatic surfaces was examined, revealing potential points that enhance the binding affinity between CSNPs and RBD. Mutations of the potential residues were constructed with all possible combinations considering the available volume, surface complementarity, total binding energy, and stability of the complex. The resulting peptides database (81mutants) with single substitutions and their respective binding-affinities and binding stabilities were recorded and utilized in the next round of residues scan. The top five substitutions of each residue (*i.e.*, Glu23, Lys26, Thr27, His34, and Gln42) were selected and implemented in the multi-substitution peptides construction step. Monitoring their binding energies could identify several best fit peptides to the RBD interface (Table S1). Residues substitution in CSNP2 evenly distributes the hotspots and exhibits stronger affinity than CSNP1 (Fig. S1B). To retain the helicity, we developed a structural constraint (lactam amide bond) between the side chains of the non-interface residues Phe32Asp and Ala36Lys. A shorter constrained peptide, CSNP3, was constructed by considering the pharmacophores of α1 helix to validate the

importance of Lys353 and the self-sufficiency of α1 helix for RBD binding. Four non-constrained derivatives (Pep2, Pep3, Pep4, and Pep5) of the CSNP3 were designed for comparative binding affinity analysis. All peptides are listed in table S2, providing their properties and differences.

The fourth peptide CSNP4 was designed by considering the spontaneous position switching and ACE2-RBD interface residues of the RBD. Two amino acid stretches of 445–456 and 488–501 that participate in ACE2 binding were truncated from the RBD and joined through a flexible linker Gly-Arg-Gly-Pro (GRGP) to orient the optimal peptide joining and retain its target-binding ability. In its resting position (RBD^{down}), the same sheet-loop-sheet motif (CSNP4) lies between the NTD and the RBD domains of the adjacent S protomer (Fig. S1D), as shown previously [24]. Thus, we propose that in addition to ACE2-RBD hindrance, CSNP4 may restrict the spontaneous position switching of RBD and pose its crucial epitopes for immune surveillance.

3.2. Structural constraints stabilize the CSNPs

Structural stability and resistance to enzymatic degradation are essential aspects that need to be considered while designing small therapeutic peptides. Moreover, fold-on-binding requires time, and often peptides lose their target-specificity upon unfolding [35]. Therefore, we restrained the structures of CSNP1, CSNP2, and CSNP3 by applying structural constraints and joined the two amino acid stretches of the CSNP4 through a shorter loop "GRGP". The structural stability of the CSNPs was investigated by simulating them in an aqueous environment as a function of time. We also simulated SBP1 as a control case, a previously reported structurally unrestrained ACE2-derived RBD-binding peptide [23]. Overall, we observed a considerably large root mean square deviation (RMSD) in all peptides in the second and third quarters of the simulation (Fig. 2A), suggesting that the peptides have undergone energy transition and acquired a low energy state during the simulation. To track down the fluctuation of RMSD, we calculated the root mean square fluctuation (RMSF) of all atoms of the peptides. The terminal atoms of all peptides, particularly in CSNP4, exhibited considerable fluctuation compared to the atoms in peptide bodies. However, CSNP1 and SBP1 showed high fluctuation in atoms ranging from 100 to 170 compared to CSNP2 or CSNP3 (Fig. S2A). The atoms ranging from 154 to 165, corresponding to Asp30 in CSNP1 and SBP1, are crucial amino acids contributing to the ACE2-RBD interface. This suggests that the Lactam Bridge in CSNP2 and CSNP3 stabilize these amino acids by retaining their helicity. In addition, SBP1 and CSNP3 showed a diminished radius of gyration (Rg), which predicts the folding with the compactness of the peptides, indicating structural shrinkage with dramatic shift (Fig. S2B). This result suggests that the hydrogen bonds between the sidechains of these peptides probably acquire a new pattern disordering the peptide structures. To validate these data, we extracted 1000 structural frames from the 200 ns MD trajectory of each CSNP and investigated their secondary structural alteration (**Movie S1**). Remarkably, we observed that CSNP1 and SBP1 were shifted from helical to irregular looped structures, permanently losing their helicity; however, CSNP3 partly retained its helical structure. CSNP2 holds an intact structure, but its C-terminal S-S constraint region remained flexible at the PGG junction (Fig. 2B). These data suggest that structural constraints stabilize peptide helicity and retain their target binding affinity.

3.3. Molecular dynamcis simulation and free energy perturbation of the target-bound peptides

ACE2-derived CSNPs, docked onto RBD, were simulated in a neutralized solution state, whereas CSNP4 was simulated with ACE2. All the target-bound peptides were relatively more stable as compared to their unbound isolated states (Fig. S2C). However, CSNP3 exhibited an increased RMSD (Fig. S2D) due to the N-terminal hydrophilic Glu1 that detaches RBD during simulation

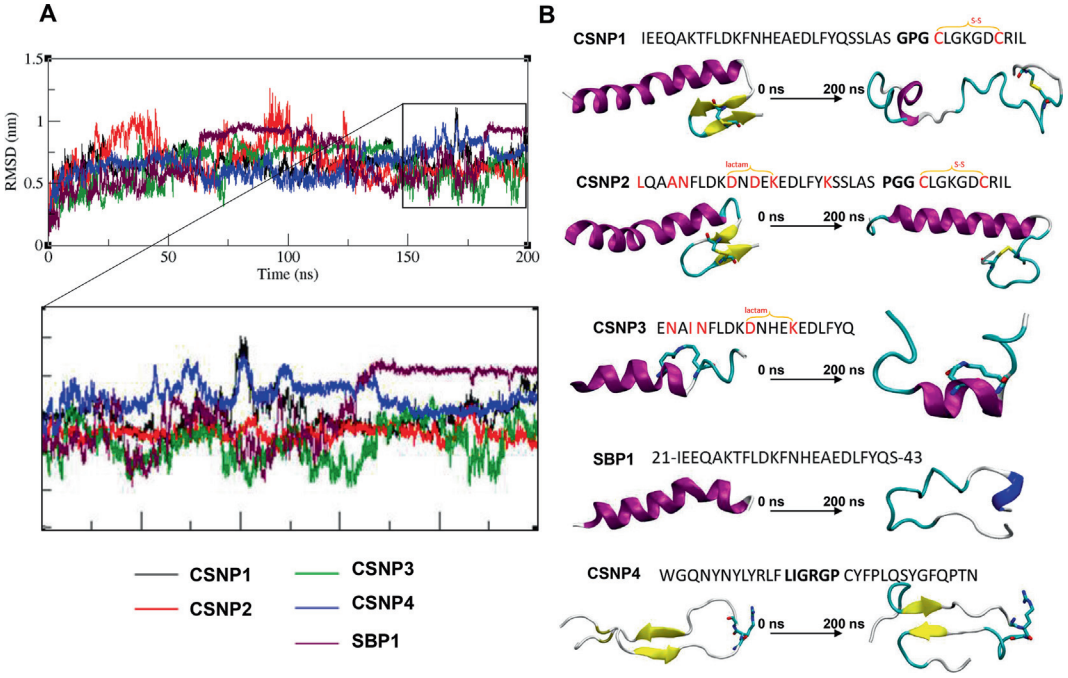

Fig. 2. Structural validation of the SARS-CoV-2 Spike inhibiting peptides (CSNPs). A) Root mean square deviation (RMSD) plots of all atoms in CSNPs and SBP1. The color codes are shown at the bottom. The last 50 ns trajectory is enhanced for clarity. B) The representative 3D structures of the CSNPs and SBP1 peptides show a significant shift in their structure as they evolve during simulation. The structural coordinates were taken from the first and last nanosecond of the MDS trajectory. The purple color represents helicity, cyan represents loop, and the yellow color corresponds to β-sheets. CSNP1 and CSNP3 undergo a drastic shift in structure. The real-time changes in the secondary structures are shown in Movie S1. (For interpretation of the references to color in this figure legend, the reader is referred to the web version of this article.)

(**Movie S2**). SBP1 also increased the overall RMSD of RBD, similar to that of CSNP3-RBD. The interface residues of the docked CSNPs overlapped with those of ACE2-RBD (Table 1 vs. Tables S3 & S4); nonetheless, some of these interactions shifted during MDS.

To measure the dissociation of CSNPs from their targets, we calculated the average distances between the centers of their masses (Fig. S2E) and monitored the inter-chains hydrogen bonds number as a function of time (Fig. S2F). The average interaction distance of the CSNP1-, CSNP2-, and SBP1-RBD complexes remained constant during simulation; however, the distances between CSNP3 and RBD were unstable (Fig. S2D). The distance between the center of masses of CSNP4 and ACE2 was ~ 35 nm at the start of MD simulation and increased up to ~ 40 nm at the midpoint [50] (Fig. S2E). This discrepancy could be explained by the free N- and C-terminals of CSNP4, which affected the overall stability of CSNP4 and may have similar impact on the CSNP4-ACE2 complex. The distance of CSNP3-RBD fluctuated due to the loosely bound hydrophilic N-terminal Glu1 of the peptide, affecting the adjacent Asn2 to detach RBD (see **Movie S2**). This detachment compels the N-terminal of CSNP3 in a whip-like motion; nonetheless, the C-terminal residues remained intact with RBD.

Next, the binding strength of the peptides with their targets was estimated using MMPBSA and molecular mechanics generalized Born model and solvent accessibility (MMGBSA) methods, calculating van der Waals (vdW), Electrostatic (Ele), Polar Solvation (PS), and Solvent accessible surface area (SASA) energies of the peptide-bound complexes (Table 2). CSNP1 and CSNP2 showed similar overall binding affinities to RBD (CSNP1, total E = -298.44 +/− 47.17 kcal/mol; CSNP2, total E = -283.77 +/− 56.39) (Fig. 3A), although CSNP2 exhibited stronger vdW and Ele energies than CSNP1 (Table 2). CSNP3 exhibited relatively stronger total binding energy with RBD (total E = -382.73 +/− 63.4 kcal/mol) than that of SBP1 (-356.73 +/− 75.1 kcal/mol); nonetheless, the polar solvation energy of SBP1 remained higher than CSNP3 which is inversely correlated with the electrostatic potential (Table 2). One limitation of the in silico free energy perturbation is that these tools do not take the unbound solution state of a peptide into account, and the calculated energy terms result from a difference in energies of the amino acids involved at the interface vs their theoretically unbound state. As we observed that SBP1 loses its structure in solution (see **Movie S1**), one can expect delayed or no binding with RBD. On the contrary, SBP1/RBD exhibits stronger Ele potential and high polar solvation energy than the constrained CSNPs, suggesting its slower dissociation.

The accumulation of multiple mutations in the Spike has increased the virus's infectivity and pathogenicity, acquiring resistance to neutralizing antibodies [53]. To date, more than 15 mutations have been reported in the Spike's RBD, where most of these mutations are located in the receptor-binding motif (RBM) (Fig. 3B) and enhance the receptor-binding capacity of the virus [53–54]. Omicron (BA.1 and BA.2 clades) contains at least 15 mutations in the RBD region and escapes most of the FDA-approved antibody-based drugs formulated by Regeneron, AstraZeneca, AbCellera, and other companies [15,17]. CSNP1 and CSNP2 were derived from the α-helix of ACE2 that bind RBD; therefore, we speculated whether the mutations in RBD affect the peptides' binding affinity. Considering peptides as ligands and RBD as a receptor, we calculated the end-point binding affinities (MMGBSA) of the peptides with all VOCs. CSNP1, which has not been modified from its original structure, reduced its binding with Beta and Gamma variants and increased its affinity towards Alpha and Omicron variants. In contrast, CSNP2 showed increased binding affinities with all VOCs (Fig. 3C). These data suggest that if mutations in the RBD persist/arise, peptides drugs designed *de novo* or rationally by modifying the α1 helix of ACE2 may show different efficacy. To validate the MMGBSA-based binding free energy terms, we simulated CSNP1 and CSNP2 with $RBD^{Omicron}$ and calculated the binding free energy terms using the MMPBSA approach. Similar to MMGBSA values, CSNP1 and CSNP2 showed more potent binding energies with $RBD^{Omicron}$ than $RBD^{W.T}$ (Fig. 3D, E). Since viruses adapt to their host and enhance their binding with the same ACE2 receptor, we suggest that CSNP1 and CSNP2 could be potent therapeutic candidates to cope with the continuously mutating Spike.

3.4. Biophysical interaction between peptides and target proteins (SPR)

SPR measures the binding kinetics and biophysical interactions of biomolecules and is thought to be more reproducible and sensitive than Biolayer interferometry [55–56]. Initially, we immobilized ACE2 and S1 to the CM5 sensor chip as the ligands and cross-tested them as analytes. The K_D was 3.66 nM when S1 was immobilized as ligand, and ACE2 was used as an analyte. Nonetheless, when ACE2 was immobilized to the chip as a ligand and S1 was used as an analyte at different concentrations, the K_D was increased 5-fold (K_D = 17.42 nM, Fig. S3). Although these data demonstrated the complementarity of S1-ACE2, the difference in K_D could be due to the experimental conditions of assay or ligand and analytes switching for amine-coupling.

Next, we treated CNSP1-4 and Pep1-5 as analytes in the immobilized S1 and calculated their binding kinetics (Fig. 4A). CSNP1, CSNP2, and CSNP4 exhibited a dose-dependent binding to S1 subunit (Fig. 4B-D). The relatively shorter CSNP3 peptide and its derivatives Pep2-5 did not show any binding (Fig. S4); however, an un-modified linear peptide Pep1 exhibited moderate binding with S1 (Fig. 4**E**). We synthesized the peptides from two commercial facilities GL-Biochem and Peptron Inc (see methods) and compared the binding kinetics for CSNP4 from the two different sources. $CSNP4^{Peptron}$ showed multiple on and off-rates and the K_D was recorced as 1.2 μM, where the curves did not fit well in different concentrations (Fig. S5). By contrast, $CSNP4^{GL}$ exhibited a dose-dependent binding to S1 with ideal off- and on-rates and fitted well at different concentrations (K_D = 0.14 μM), suggesting that factors such as experimental techniques and peptides synthesis procedures can affect the peptides-target binding kinetics and require further validation. The S1-ACE2 binding was relatively stronger (K_D = 3 to 17 nM) than the CSNP1-RBD binding, which might be due to the enhanced binding by the α1 helix with the

Table 2
Binding free energy of the CSNP-bound ACE2 and RBD complexes.

Complex	VDW E	Ele E	PS E	SASA E	Total E
CSNP1/RBD	−294.49 +/− 26.0	−685.26 +/− 74.0	719.22 +/− 125.0	−37.91 +/− 3.3	−298.44 +/− 82.0
CSNP2/RBD	−302.45 +/− 20.3	−705.56 +/− 96.1	763.25 +/− 119.8	−39.01 +/− 2.4	−283.77 +/− 81.3
CSNP3/RBD	−225.15 +/− 26.6	−660.4 +/− 159.4	532.67 +/− 190.2	−29.85 +/− 4.3	−382.73 +/− 63.4
SBP1/RBD	−282.12 +/− 23.7	−889.03 +/− 74.0	853.42 +/− 116.0	−39.00 +/− 2.4	−356.73 +/− 75.1
CSNP4/ACE2	−217.30 +/− 29.6	−1124.5 +/− 72.6	422.46 +/− 135.8	−27.72 +/− 3.4	−947.06 +/− 104.2

VDW: van der Waal; Ele: Electrostatic; PS: Polar Solvation; SASA: Solvent accessible surface area; E: Energy. All energies are measured in kjol/mol.

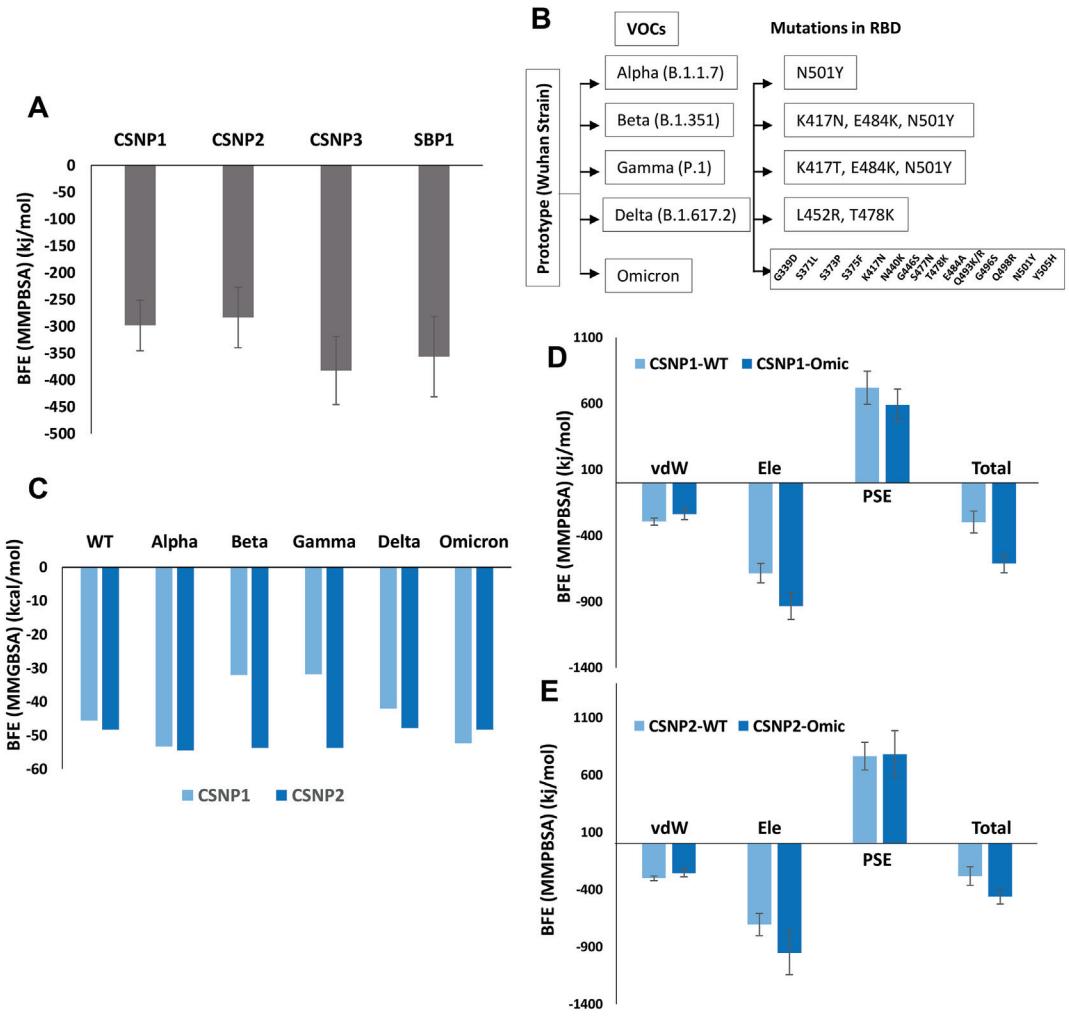

Fig. 3. The binding free energy perturbation of the CSNPs with RBD of SARS-CoV-2 VOCs. **A**) Binding free energy of RBD^{WT} against CENPs and SBP1 calculated through MMGBSA. **B)** The SARS-CoV-2 variants of concerns and individual mutations in the RBD domain. Binding free energy calculated through MMGBSA between CSNP1 and CSNP2 and all SARS-CoV-2 VOCs. **C)** Relative change in the binding free energy of CSNP1 and CSNP2 when bound to RBD^{WT} and $RBD^{Omicron}$.

Lys353 and the auxiliary residues of the ACE2-RBD interface (Table 1).

We also evaluated the binding kinetics of CSNP4 with the immobilized ACE2, revealing relatively weak and dose-dependent binding affinity (K_D = 158 μM) (Fig. 4F,G). The weak binding affinity of CSNP4-ACE2 can be explained by other reasons. The α1 helix of ACE2 provides a narrow and shallow surface for the CSNP4 binding, weakening the binding affinity. Moreover, CSNP4 does not have Lys417, which contributes to ACE2-RBD binding (see Table 1). The ACE2-binding motif on RBD (RBM) has a large conformational space and irregular loop structure; thus, it may not be appropriate to design an RBD-derived decoy peptide that blocks the ACE2-RBD interaction. However, amino acid stretches in the RBM have elicited anti-SARS-CoV-2B- and T cell responses [57–58]. We could demonstrate that FITC-tagged CSNP4 home around human ACE2 (hACE2) overexpressing cells (hACE2-293T) by immunocytochemical analysis, whereas FITC-CSNP1 did not show such effect (Fig. S6). We also confirmed that this effect was not due to the peptide aggregation, but CSNP4 exhibits a better binding tendency towards ACE2 when expressed on the cells. Thus, CSNP4 may neutralization SARS-CoV-2 by two ways: one due to the strong CSNP4-S1 binding and second due to its homing ability to hACE2-expressing cells.

3.5. CSNPs neutralize SARS-CoV-2 Spike pseudovirus and interfere with the S1-hACE2 binding.

To assess the safety and anti-SARS-CoV-2 efficacy of selected peptide candidates, we established the hACE2-293T-pseudovirus system (Fig. S7A). None of the peptides showed toxicity in the hACE2-293T cells when treated at different concentrations (Fig. 5A). Next, unmodified 293T cells and hACE2-expressing 293T cells were infected with vesicular stomatitis virus G (VSVG) protein-expressing lentivirus particles and SARS-CoV-2 wild-type Spike pseudovirus ($pseudovirus^{WT}$). VSVG-expressing viral particle effectively infeced the ACE2 lacking 293T cells, but $pseudovirus^{WT}$ did not show any signlas (Fig. 5B, *top*). By contrast, $pseudovirus^{WT}$ effectively infected the hACE2-293T cells (Fig. 5B, *bottom*). Next, the inhibitory effect of peptides was investigated against $pseudovirus^{WT}$ in a NanoLuc luciferase reporter assay, which has been known to accurately predict the SARS-CoV-2 neutralization of mAbs [59–60]. We observed that CSNP1, CSNP2, and CSNP4 inhibited the Luciferase activity and were concentration-dependent, whereas Pep1 had a moderate effect (Fig. 5C).

CSNP2 ($IC50^{WT}$ = 0.37 μM) and CSNP4 ($IC50^{WT}$ = 0.35 μM) could inhibit up to 80 % of Luciferase activity when treated at 0.5 μM, whereas CSNP1 (IC50 = 30 μM) could inhibit ~ 50 % of the activity

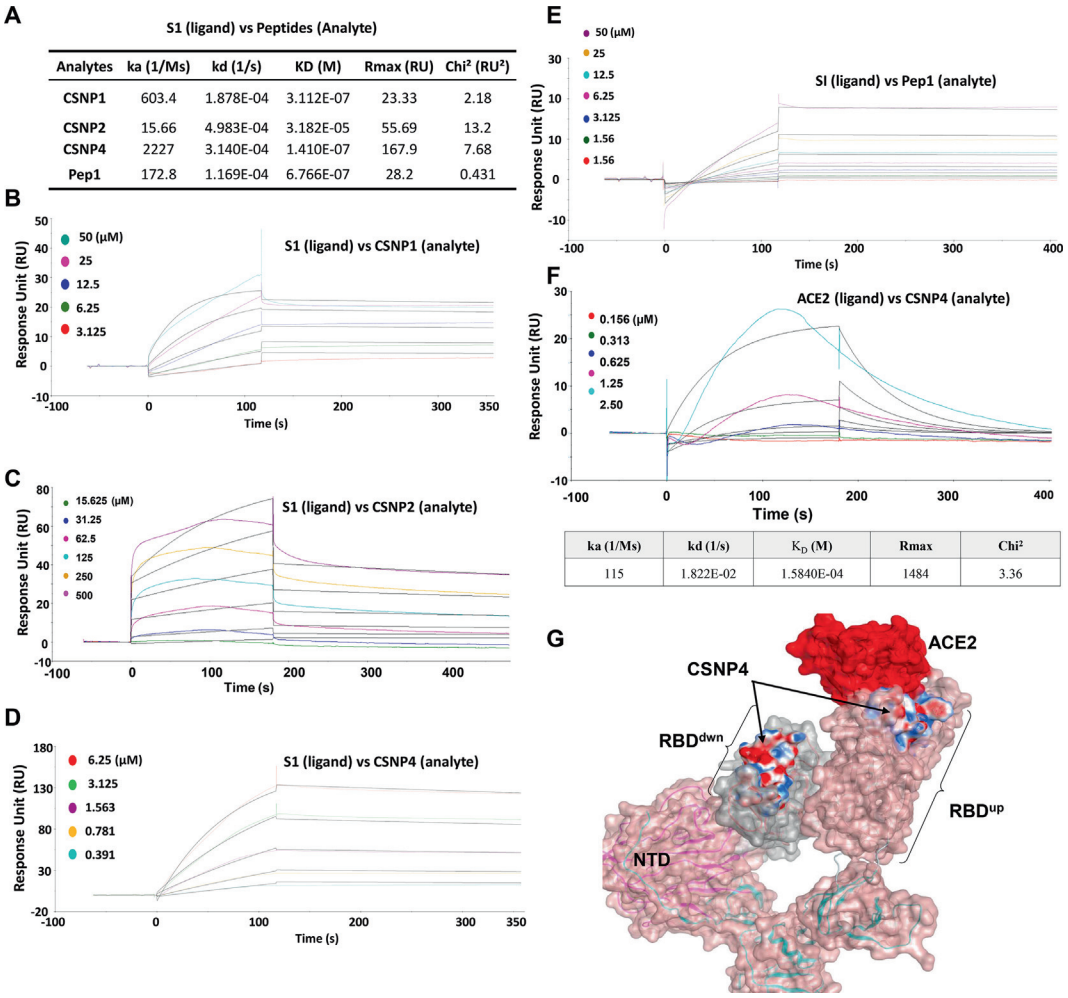

Fig. 4. The binding kinetics of the hACE2, SARS-CoV-2 S1, and CSNP peptides. A) The binding affinities of S1 and hACE2 to CSNPs were determined by immobilizing both proteins to the chip in separate channels. The sensorgrams showing 1:1 binding are shown, and their association (ka) and dissociation (kd) rates and equilibrium constants of dissociation K_D are given in the tables below (A). A-E) Helical peptides CSNP1, CSNP2, and Pep1 bind S1 protein dose-dependently. F) CSNP4 binds dose-dependently. The K_D values are in the table below, and the target binding mechanism of CSNP4 is depicted as a cartoon (panel C). C) CSNP4 binds to ACE2 when the Spike RBD acquires "up" conformation and binds to Spike between the NTD and RBD "up" of the adjacent Spike protomer.

at the same concentration. This finding was surprising as CSNP1 had K_D = 0.31 μM, which is ~ 100 fold stronger than CSNP2 (KD = 32.8 μM) in the SPR assay (Fig. 4A). This discrepancy between the SPR and experimental data could be explained by the fact that CSNP2 is constrained by a lactam amid bridge and a disulfide bond, whereas CSNP1 has a single disulfide bond as a structural constraint. Besides, CSNP2 holds its structure and perhaps readily binds RBD compared to CSNP1 as suggested by the MD data, which may consume extra time for refolding in solution and target-binding. Similarly, Pep1 does not contain any structural constraints and exhibited relatively lower pseudovirus^{WT} inhibition than CSNP1 (Fig. 5C). Although CSNP3 did not bind the S1^{WT} domain of Spike in SPR assay, we investigated whether it could inhibit the pseudovirus^{WT} *in vitro*. Unexpectedly, we found that, unlike CSNP1, CSNP2 and CSNP4, CSNP3 did not inhibit the pseudovirus^{WT} activity at 0.01 μM but did show some effect at higher concentrations. However, this effect was not dose-dependent (Fig. S7B). To further confirm this effect, CSNP3 was co-treated with the S1^{WT} domain in hACE2-293T cells and compared the outcomes with CSNP2 and CSNP4. We found that CSNP2 and CSNP4, but not CSNP3, completely abolished the S1-ACE2 interaction, as confirmed by the localization of S1 to the ACE2 through immunocytochemistry analysis (Fig. S7C). We also evaluated the effect of the CSNPs in the β-catenin labeled hACE2-293T cells to track the membrane (in other words, hACE2) localization of S1, because β-catenin is strongly expressed by the 293T cells and is used to localize the expression of other proteins such as N-Cadherin [61]. As expected, CSNP2 and CSNP4 fully blocked the membrane localization of S1, but CSNP3 did not show such an effect (Fig. S7D). This suggests that reduction in the peptides size and custom modification could have off-target effects that may undermine the legacy of peptide-based therapeutics. Hence, optimum length and crucial pharmacophore in a therapeutic peptide are vital to guarantee target-specificity and therapeutic efficacy.

3.6. CSNPs inhibit all SARS-CoV-2 VOCs pseudoviruses, including Delta and Omicron

To check whether CSNPs hold a pan-variant inhibitory effect, we constructed pseudovirus particles expressing Spike proteins of the reported SARS-CoV-2 VOCs, including Alpha, Beta, Gamma, Delta, and Omicron. CSNP1 neutralized over 50 % of α, β, γ, and δ pseudovirus activity when treated at 10 μM concentration, and all but γ variants were substantially inhibited at 1 μM (Fig. 6A). SARS-CoV-2 β and γ variants vary by one residue in their RBD, where the β variant contains K417N and the γ variant contains

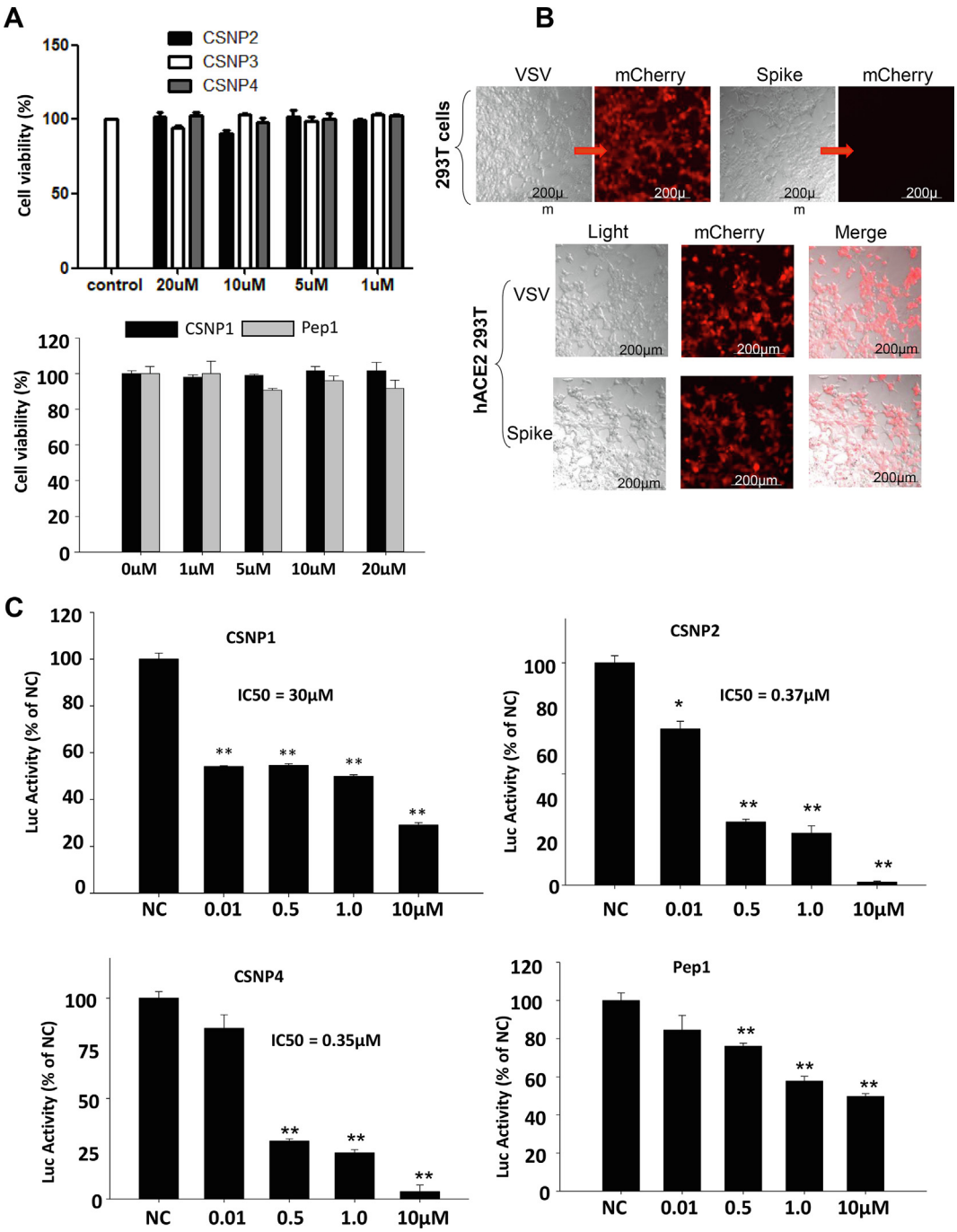

Fig. 5. CSNPs peptides deter the SARS-CoV-2 S1 and hACE2 interaction and neutralize pseudovirus infection in hACE2-293T cells. A) Cells were treated with peptides, and cell viability was measured after 48 h through cell titer blue assay. (Student's t test was used to compare differences between two groups. *P < 0.05, **P < 0.01 vs. NC groups). B) Fluorescence microscopy image of SARS-CoV-2 Spike pseudovirus infection in 293T (top), hACE2-293T cell (bottom) (scale bar = 200um). The hACE2-293T cells were infected with Spike expressing pseudovirus particles. Lentivirus expressing VSV-G surface proteins were used as a positive control. (C) The Spike^{WT} pseudovirus infected hACE2-293T cells are treated with Pep1 and CSNPs at varying concentrations (0.01, 0.5, 1, and 10 μM), and their luciferase reporter activities are measured. Statical significance is estimated using Student's t test. *P < 0.05, **P < 0.01 vs. NC groups. Statistical significance was analyzed using SigmaPlot v12.5 software (Systat Software, Inc.). All experiments were performed in triplicate, and the data are presented as the mean ± standard deviation. (For interpretation of the references to color in this figure legend, the reader is referred to the web version of this article.)

K417T (Fig. 3B). Since both Asparagine (Asn) and Threonine (Thr) are polar amino acids and do not participate in CSNP1 binding directly, a relatively lower response of γ variant at a lower dose of CSNP1 may require further insights. Nonetheless, all four variants were equally inhibited by CSNP4 in a dose-dependent manner (Fig. 6B). Unfortunately, CSNP2 was fully consumed at the stage, and we could not investigate its pan-variant inhibitory effect; however, Pep1 showed some response at 10 μM (Fig. 6C). We further investigated a dose-dependent response of the CSNP1 ($IC50^{Delta}$ = 18 μM) and CSNP4 ($IC50^{Delta}$ = 0.2 μM) against δ variant to determine its IC50 and found substantial (Fig. 6D) but relatively less effective as compared to WT strain (Fig. 5C). Finally, CSNP1, CSNP4, and Pep1 were tested against Omicron pseudovirus. All three peptides inhibited more than 50 % Luciferase activity at 10 μM

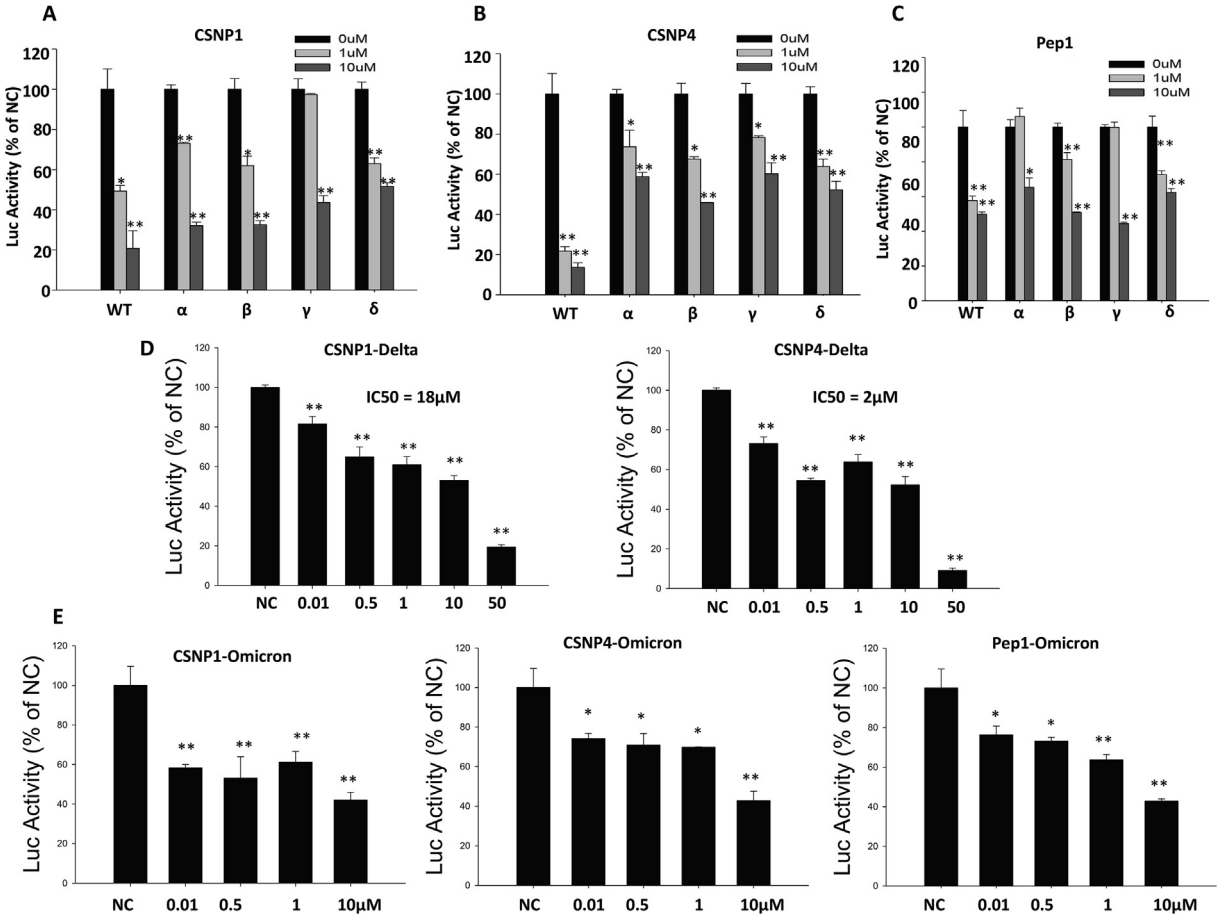

Fig. 6. CSNPs inhibit all SARS-CoV-2 variants of concerns (VOCs) pseudovirus infection in hACE2-293T cells. **A, B, C)** The luciferase reporter activity was measured for the Spike^{WT}, Spike$^{\alpha}$, Spike$^{\beta}$, Spike$^{\gamma}$, and Spike$^{\delta}$ pseudovirus infected hACE2-293T cells when treated with 1, and 10 μM of CSNP1 or CSNP4 or Pep1. **D**) Similarly, a dose-dependent response was measured for CSNP1 and CSNP4 against Spike$^{\delta}$ pseudovirus. **E**) The luciferase reporter activity was measured for Spike^{Omic} pseudovirus against CSNP1 and CSNP4. The Student's t test was used to compare the differences between the two groups. *P < 0.05, **P < 0.01 vs. NC groups. Statistical significance was analyzed using SigmaPlot v12.5 software (Systat Software, Inc.). All experiments were performed in triplicate, and the data are presented as the mean ± standard deviation.

and ~ 40 % at 1 μM concentration (Fig. 6D). These data confirm that CSNPs, particularly CSNP2 and CSNP4 are SARS-CoV-2 pan-variant inhibitory candidates and hold promise in COVID-19 therapy in the long run, particularly when drug-resistant and immune-escaped variants are pouring into a population.

3.7. CSNPs are self-synergizing and reinforce the effect of non-overlapping RBD-neutralizing mAbs.

So far, hundreds of mAbs, polyclonal antibodies, and Spike-neutralizing synthetic antibodies (nAbs) have been reported that recognize various epitopes on the Spike's S2, NTD, and RBD domains [62–64]. To demonstrate whether CNSP1 or CSNP2 compete with the RBD neutralizing mAbs, we collected 642 mAbs that bind and neutralize only the RBD region of the SARS-CoV-2 Spike. Among them, we selected 105 non-identical mAbs, which were structurally resolved with SARS-CoV-2 Spike and their structures were available in the RSCB PDB database (https://www.rcsb.org, Supplementary Raw data (mAbs)). These mAbs were clustered by the CDRH3 regions (CDRs were designated according to the IMGT scheme) [65] through a phylogenetic tree using Clustal Omega [66]. We could roughly stratify the CDRs into non-overlapping, partially overlapping, and fully overlapping RBD interfaces for CSNP1 and CSNP2, although the idea was less robust as five CDRs including CDRL3 were excluded from the phylogenic analyses (Fig. S8A). Interestingly, we found that mAbs such as bamlanivimab (PDB ID: 7KMG) that neutralize the D614G and Alpha but not Beta and Delta and imdevimab (REGEN-COV from Regeneron pharmaceuticals) that neutralizes all SARS-CoV-2 variants [67] do not overlap or clash with the binding of CSNP1 and CSNP2 on RBD. In addition, BG10-19 and BG1-24 nAbs are known to lock the RBD in its closed conformation and neutralize the Alpha and Beta variants of SARS-CoV-2 [68]. We demonstrated whether CSNPs can hinder nAbs that neutralize the RBD in its closed conformation. By superimposing the CSNP1/2-RBD complex over the Spike-BG1-24 complex containing two close and one open RBD, we could demonstrate that CSNP1/2 freely binds the open RBD and occupy the free cavity of closed RBD without making any clash with nAbs (Fig. S8B). Furthermore, Ju et al. have identified 206 ACE2-competing RBD-specific mAbs from eight SARS-CoV-2 patients [63]. We found that CSNP2 could not make any steric hindrance with P2B-2F6 that binds the RBD in its open conformation (Fig. S8D). Thus, we suggest that CSNP1 and CSNP2, which binds to the same RBD interface, may interact with both open and closed RBD, abrogating the ACE2-RBD interaction and allowing RBD to be recognized by the neutralizing antibodies.

To confirm this notion, we experimented whether CSNP1 and CSNP4 are mutually synergistic and aid into the neutralizability of CR3022 antibody, which recognizes a conserved epitope on both SARS-CoV-1 and SARS-CoV-2 and moderately neutralizing SARS-CoV-2 [57,69]. By superimposing the CR3022 and CSNP1/2 onto the same RBD, we could see that mAb recognizes a conserved epi-

tope that we predicted during the early course of the COVID-19 pandemic [24] and does not overlap with CSNP1/2 (Fig. 7A). In our Delta variant pseudovirus assay, CR3022, CSNP1, and CSNP4 could independently inhibit ~ 40 % of the activity at suggested concentrations. When CSNP1 or CSNP4 were co-treated with CR3022, we could see moderate synergy in pseudovirus neutralization, but no competitive binding (Fig. 7B). Surprisingly, CSNP1 and CSNP4 together showed a substantial synergy and inhibited ~ 80 % of the pseudovirus activity at a combined 1 μM concentration. These data suggest that CSNPs peptide cocktail or CSNPs together with mAbs with no overlapping epitopes could be an effective therapeutic strategy against COVID-19.

Finally, to investigate whether CSNPs resist the enzymatic degradation, we performed a comparative proteinase K (ProtK) digestion of the CSNP1, CSNP4, and Pep1 peptides. ProtK predominantly cleaves the peptide bond adjacent to the carboxyl group of aliphatic and aromatic amino acids and thoroughly digests the protein upon prolonged incubation and high concentration. Upon investigation, we found that CSNP1 and Pep1 peptides contain two "LF" and "FL" pairs, while CSNP4 contains only one such aromatic-aliphatic amino acid combination. This could be why ProtK readily digested CSNP1 and Pep1 while CSNP4 resisted the enzymatic degradation for 60 min (Fig. 7C, D). Peptides containing D-form amino acids are resistant to enzymatic degradation and hold promising therapeutic potentials due to their extended serum half-lives [70]. Substituting terminal or all amino acids in CSNPs, particularly CSNP1 and CSNP2, into D-form may significantly enhance their half-lives while structural constraints retain the structures.

4. Discussion

Host cell entry is the first step in viral infection and remains a priority concern for therapeutic intervention. The impulsive conformation switching of the SARS-CoV-2 RBD reported by Wrapp *et al.* [3] is one of the immune evasion strategies utilized by CoVs [4,71]. ACE2 is a primary Spike recognition receptor in membrane-bound ($ACE2^{M}$) and soluble forms ($ACE2^{s}$). Watson *et al.* have demonstrated that $ACE2^{S}$ binds to RBD with a relatively similar binding affinity as its neutralizing antibodies [72]. Hence, $ACE2^{S}$ is a "double-edged sword", exhibiting a potent inhibitory action against pseudotyped lentivirus *in vitro* [73] but abrogating the neutralization of RBD. $ACE2^{S}$ has also been used to block viruses from entering cells due to its RBD-binding ability [74]. Collectively, RBD spontaneously switches from 'up' to 'down', and $ACE2^{S}$ shields the Spike protein from immune surveillance. This paradox should be considered in developing therapeutic agents that abolish the Spike-ACE2 interaction. With this concern, biologics that interfere with RBD-ACE2 binding, facilitating the "up" conformation of RBD, and minimally interfere with the antibody binding and B cell response to the S protein are required. This strategy was partly utilized by the two FDA-approved RNA-based vac-

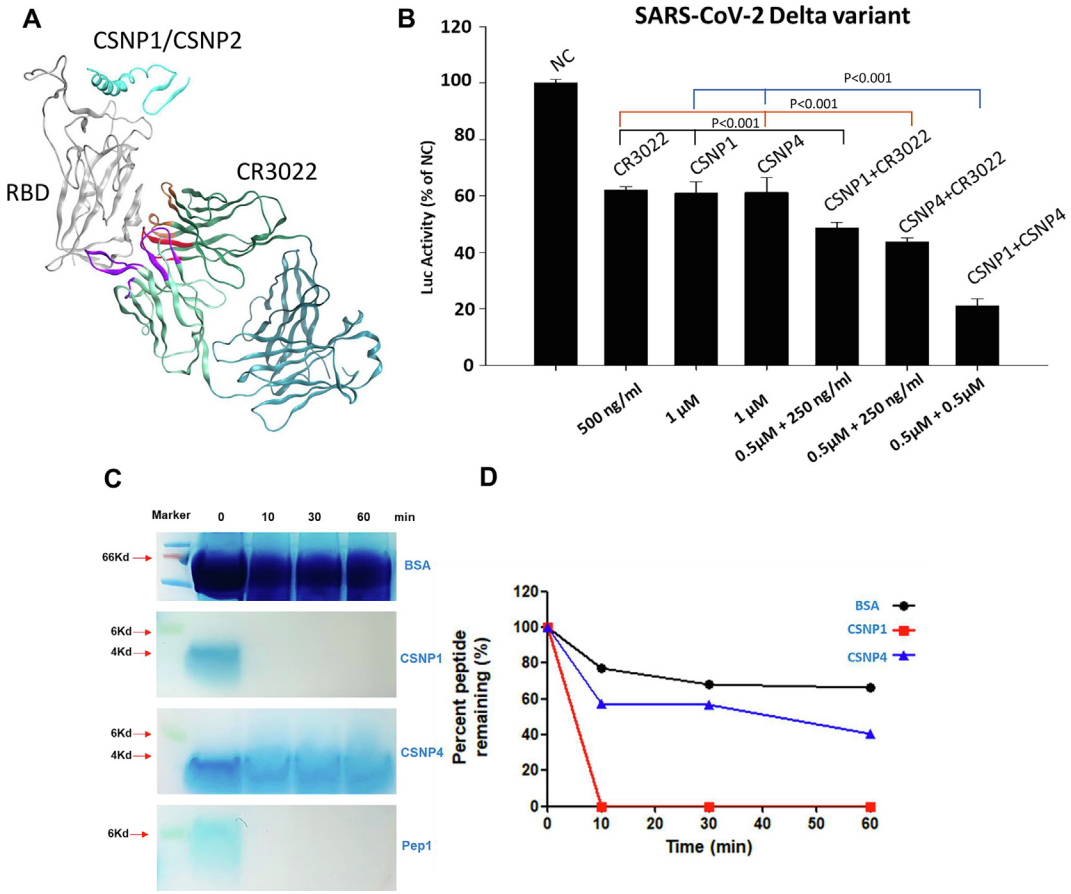

Fig. 7. CSNPs are self-synergizing and aid the neutralization of CR3022. **A)** CSNP1 and CSNP2 do not compete with CR3022 on RBD. **B**) The luciferase reporter activity was measured for $Spike^{Delta}$ pseudovirus against CSNP1, CSNP4, and CR3022 alone or in different combinations. The differences between the mean values among the treatment groups are greater than would be expected by chance (P = 0.008, Shapiro-Wilk one-way ANOVA Normality Test). All experiments were performed in triplicate, and the data are presented as the mean ± standard deviation. **C)** Peptides and bovine serum albumin (BSA) were treated with ProtK over 60 min, and the Gels were stained with Coomassie Brilliant Blue dye. **D**) Quantification of remaining BSA, CSNP1, and CSNP4 peptides bands post-ProtK treatment were determined using ImageJ software with background subtraction.

cines, BNT162b2 and mRNA-1273, that encode the SARS-CoV-2 Spike protein in a stable prefusion conformation. In both vaccines, the antigenic Spike 'S 2P' muteins are generated by substituting the two subsequent Lys986 and Val987 at the top of the central helix in the S2 domain into a Proline, converting the metastable prefusion conformation into a stable prefusion state [18]. This Spike mutein resists the enzymatic cleavage at the S1/S2 junction and expresses the RBD, containing crucial Spike neutralizing epitopes, in a stable 'up' conformation for continuous immune surveillance [75–76].

The Spike-ACE2 binding and the subsequent conformational rearrangements of the S2 for the viral-host membranes fusion are major targets for vaccines and drug development. Other researchers and we have shown that SARS-CoV-2 utilizes shallow and expanded surface contacts between Spike and ACE2 for host cells entry [3,20,24–25]. These hurdles, *i.e.*, the shallow, widely expanded, and flat contact surfaces, make the Spike-ACE2 a challenging target for widely utilized small organic molecules-based medicinal chemistry approaches. Thus, although tremendous progress has been made in targeting viral proteases with small molecules [77–78], disrupting the Spike-ACE2 interface with the same strategies remains daunting. As an alternative, small peptides, peptide-memetic, and mini-proteins have overcome these difficulties, showing remarkable outcomes in blocking viral entry and neutralization [51–52,79]. Thus, the deployment of peptide-based biologics has expanded the concept of druggability by specifically and effectively targeting PPIs that are hard to target by organic molecules [80].

SARS-CoV-2 exhibited a relative evolutionary stasis during the first year of the pandemic, whereas new variants have been continuously pouring as the virus began to evolve since late 2020. These VOCs are described as rapidly transmissible, immune evading, and more pathogenic in some cases, probably due to the variable immune profile of the host population as the virus spreads across the globe. The swift failure of the therapeutic interventions against VOCs has put the fate of COVID-19 therapeutic mAbs and nAbs and vaccines in danger. Hence, pan-variant inhibiting therapeutics are the need of the day to combat the rapidly evolving virus. Therefore, we suggest that CSNPs are promising therapeutic candidates as they inhibit all VOCs dose-dependently (Figs. 5 & 6).

Many redundant yet overlapping epitopes on the SARS-CoV-2 RBD recognized by neutralizing antibodies have been reported [62–64]. Using comparative structural analysis of antibody-antigen, we observed that CSNP1 and CSNP2 may not compete with RBD neutralizing mAbs that bind the non-RBM epitopes (Fig. S7). This suggests that the non-bulky but structurally stable CSNP1 and CSNP2 can inhibit ACE2-RBD interaction while allowing the host-induced or injected mAb to neutralize the virus. To confirm this notion, we devised a strategy to check the synergistic effect of CSNPs with CR3022 mAb that strongly binds SARS-CoV-2 Spike with a weakly neutralization effect. In addition, as CSNP1 and CSNP2 bind the same RBM motif on RBD and CSNP4 binds at a different location, we investigated whether these peptides are mutually synergistic. CR3022 has been reported to synergize the effect of CR3014 mAbs and neutralize the CR3014-escaped SARS-CoV-1 mutants [57]. We found that CSNP1 and CSNP4 did not compete with CR3022. Interestingly, CSNP1 and CSNP4 exhibited a significant mutual synergistic effect and neutralized the pseudovirus by more than 2-fold when treated together (Fig. 7B).

Despite the considerably higher selectivity and lower toxicity than the small molecules, peptides therapeutics have limitations in the stability and bioavailability due to their shortened half-lives *in vitro* and *in vivo*. These could be overcome by improved strategies such as peptides stapling, lipid and polyethylene glycol (PEG) modification, and peptide bundles, formulating effective biologics against SARS-CoV-2 Spike protein [24,79,81]. For example, the cross-linking peptide (8P9R) with the repurposed drugs (*e.g.*, umifenovir, arbidol, chloroquine, and camostat) has been shown to suppress the SARS-CoV-2 replication and interfere with the endocytic and the TMPRSS2-mediated pathways simultaneously [82]. Previously, we and others have used peptide stapling to enhance the target specificity of therapeutic peptides [35,83]. In fact, Fiarlie and his co-workers have demonstrated that the helical-constrained compounds hold comparatively similar biological potencies in PPI as their parent proteins [84]. Considering these facts, we computationally engineered the CSNPs to block the ACE2-RBD interaction, prevented capping of the Spike by ACE2^{s}, and presented Spike proteins in their open form to host B-cell responses. Since short peptides often unfold and lose their secondary structures in the solution state when truncated from tertiary folded proteins, we examined the structural stability of the CSNPs by MDS and found that the unconstrained peptides rapidly lost their helicity and converted into irregular loops (Fig. 2, **Movie S1**). This may be one of the reasons short peptides lose target specificity.

The enzymatic resistance of CSNPs was evaluated through a ProtK digestion assay. Since ProtK holds a strong protein-digesting ability, we could observe that CSNP1 and Pep1 were readily digested while CSNP4 resisted this digestion until 60 min and beyond (Fig. 7C). Upon sequence and structure investigation, we could observe that CSNP1 and Pep1 contain two "LF" and "FL" pairs which are the potential target points of ProtK. In contrast, CSNP4 contains only one such aromatic-aliphatic amino acid combination. Peptides containing D-form amino acids resist such ProtK digestion [70]. However, other groups have reported that structurally constrained peptides (using a similar strategy as we implemented) resist serum digestion for two hours [85]. Therefore substituting terminal or all amino acids in CSNPs, particularly CSNP1 and CSNP2, into D-form may further enhance their half-lives, while structural constraints may retain the structures and target-binding affinity.

The physical stability of peptides-based therapeutic against enzymatic degradation, temperature, pressure, and aggregation remains a daunting challenge for pharmaceutics. A chemical modification would help achieve an effective plasma concentration of the CSNPs, such as the incorporation of the non-natural amino acids [86], restricting the peptides unfolding in solution by incorporating disulfide bonds [86], and stapling through lactam amide bonds [35] and hydrocarbon [85]. Also, lipidation, PEGlyation [86–87], and acylation can increase the peptides' half-life.

5. Conclusions

SARS-CoV-2 is continuously evolving and mutating its Spike protein for better host adaptation and survival; however, the primary host cells receptor, *i.e.*, ACE2, remains the same. Many antibodies derived from the convalescent plasma of the earlier COVID-19 patients and mAbs developed against the prototype Spike are gradually becoming ineffective against the mutating Spikes expressed by the SARS-CoV-2 variants. Similarly, synthetic or *de novo* Spike neutralizing peptides may lose therapeutic efficacy against mutated Spikes. However, peptide decoys such as CSNPs, derived from ACE2 or Spike proteins will effectively abolish the Spike-ACE2 interaction of emerging variants unless these decoys are considerably modified to enhance their binding to prototype Spike. We suggest that CSNP1, CSNP2, and CSNP4 are potent candidates in this regard to block the prototype and newly arising SARS-CoV-2 VOCs, including Omicron.

6. Ethical approval and Consent to participate

Not applicable.

7. Availability of data and materials

The structural data generated during and/or analyzed during the current study are available from the corresponding author on reasonable request.

8. Funding

This research was supported by grants from the National Research Foundation of Korea (NRF) funded by the Ministry of Science and ICT (MSIT) (NRF-2017M3C9A6047620, NRF-2019R1A5A2026045, and NRF-2017M3A9B6061509) and the grant from the Korea Health Industry Development Institute (KHIDI) funded by the Ministry of Health & Welfare, Republic of Korea (HI21C1003). This research was also supported by grants from the Korea Health Technology R&D Project through the Korea Health Industry Development Institute (KHIDI), funded by the Ministry of Health and Welfare, Republic of Korea (HV22C0164). In addition, this study was also supported by KREONET (Korea Research Environment Open NETwork), which is managed and operated by KISTI (Korea Institute of Science and Technology Information).

9. Authors' contributions

M.S. and H.W. conceptualized the project and designed the methodology; M.S., J.H.K., T.T.T., and S. U.M. performed the investigation and formal analysis; M.S., S.U.M., and H.W. wrote the original manuscript draft; H.W supervised the study and provided funding acquisition; all the authors contributed to editing and reviewing the manuscript.

Declaration of Competing Interest

The authors declare that they have no known competing financial interests or personal relationships that could have appeared to influence the work reported in this paper.

Appendix A. Supplementary data

Supplementary data to this article can be found online at https://doi.org/10.1016/j.csbj.2022.04.030.

References

[1] Duchene S, Featherstone L, Haritopoulou-Sinanidou M, Rambaut A, Lemey P, Baele G. Temporal signal and the phylodynamic threshold of SARS-CoV-2. Virus Evol 2020;6(2). veaa061.
[2] Worobey M, Pekar J, Larsen BB, Nelson MI, Hill V, Joy JB, et al. The emergence of SARS-CoV-2 in Europe and North America. Science 2020;370(6516):564–70.
[3] Wrapp D, Wang N, Corbett KS, Goldsmith JA, Hsieh CL, Abiona O, et al. Cryo-EM structure of the 2019-nCoV spike in the prefusion conformation. Science 2020;367(6483):1260–3.
[4] Yuan Y, Cao D, Zhang Y, Ma J, Qi J, Wang Q, et al. Cryo-EM structures of MERS-CoV and SARS-CoV spike glycoproteins reveal the dynamic receptor binding domains. Nat Commun 2017;8:15092.
[5] Mansbach RA, Chakraborty S, Nguyen K, Montefiori D, Korber B, Gnanakaran S. The SARS-CoV-2 Spike Variant D614G Favors an Open Conformational State. bioRxiv 2020.
[6] Zhang L, Jackson CB, Mou H, Ojha A, Rangarajan ES, Izard T, et al. The D614G mutation in the SARS-CoV-2 spike protein reduces S1 shedding and increases infectivity. bioRxiv 2020.
[7] Korber B, Fischer WM, Gnanakaran S, Yoon H, Theiler J, Abfalterer W, et al. Tracking changes in SARS-CoV-2 Spike: Evidence that D614G increases infectivity of the COVID-19 virus. Cell 2020;182(4):812–27 e19.
[8] Harvey WT, Carabelli AM, Jackson B, Gupta RK, Thomson EC, Harrison EM, et al. SARS-CoV-2 variants, spike mutations and immune escape. Nat Rev Microbiol 2021;19(7):409–24.
[9] Krause PR, Fleming TR, Longini IM, Peto R, Briand S, Heymann DL, et al. SARS-CoV-2 variants and vaccines. N Engl J Med 2021;385(2):179–86.
[10] Kemp SA. Neutralising antibodies drive Spike mediated SARS-CoV-2 evasion. medRxiv 2020.
[11] Faria NR, Mellan TA, Whittaker C, Claro IM, Candido DDS, Mishra S, et al. Genomics and epidemiology of the P.1 SARS-CoV-2 lineage in Manaus, Brazil. Science 2021;372(6544):815–21.
[12] Achek A, Kwon HK, Patra MC, Shah M, Hong R, Lee WH, et al. A peptide derived from the core beta-sheet region of TIRAP decoys TLR4 and reduces inflammatory and autoimmune symptoms in murine models. EBioMedicine 2020;52:102645.
[13] Wang P, Nair MS, Liu L, Iketani S, Luo Y, Guo Y, et al. Antibody resistance of SARS-CoV-2 variants B.1.351 and B.1.1.7. Nature 2021;593(7857):130–5.
[14] Madhi SA, Baillie V, Cutland CL, Voysey M, Koen AL, Fairlie L, et al. Efficacy of the ChAdOx1 nCoV-19 Covid-19 Vaccine against the B.1.351 Variant. N Engl J Med 2021;384(20):1885–98.
[15] Shah M, Woo HG. Omicron: A Heavily Mutated SARS-CoV-2 Variant Exhibits Stronger Binding to ACE2 and Potently Escapes Approved COVID-19 Therapeutic Antibodies. Front Immunol 2021;12:830527.
[16] Meng B, Abdullahi A, Ferreira I, Goonawardane N, Saito A, Kimura I, et al. Altered TMPRSS2 usage by SARS-CoV-2 Omicron impacts infectivity and fusogenicity. Nature 2022;603(7902):706–14.
[17] Cao Y, Wang J, Jian F, Xiao T, Song W, Yisimayi A, et al. Omicron escapes the majority of existing SARS-CoV-2 neutralizing antibodies. Nature 2022;602(7898):657–63.
[18] Shah M, Woo HG. Molecular Perspectives of SARS-CoV-2: Pathology, Immune Evasion, and Therapeutic Interventions. Mol Cells 2021;44(6):408–21.
[19] Lan J, Ge J, Yu J, Shan S, Zhou H, Fan S, et al. Structure of the SARS-CoV-2 spike receptor-binding domain bound to the ACE2 receptor. Nature 2020;581(7807):215–20.
[20] Shang J, Ye G, Shi K, Wan Y, Luo C, Aihara H, et al. Structural basis of receptor recognition by SARS-CoV-2. Nature 2020;581(7807):221–4.
[21] Hu H, Li L, Kao RY, Kou B, Wang Z, Zhang L, et al. Screening and identification of linear B-cell epitopes and entry-blocking peptide of severe acute respiratory syndrome (SARS)-associated coronavirus using synthetic overlapping peptide library. J Comb Chem 2005;7(5):648–56.
[22] Han DP, Penn-Nicholson A, Cho MW. Identification of critical determinants on ACE2 for SARS-CoV entry and development of a potent entry inhibitor. Virology 2006;350(1):15–25.
[23] Zhang G, Pomplun S, Loftis AR, Tan X, Loas A, Pentelute BL. Investigation of ACE2 N-terminal fragments binding to SARS-CoV-2 Spike RBD. biorxiv 2020.
[24] Shah M, Ahmad B, Choi S, Woo HG. Mutations in the SARS-CoV-2 spike RBD are responsible for stronger ACE2 binding and poor anti-SARS-CoV mAbs cross-neutralization. Comput Struct Biotechnol J 2020;18:3402–14.
[25] Yi C, Sun X, Ye J, Ding L, Liu M, Yang Z, et al. Key residues of the receptor binding motif in the spike protein of SARS-CoV-2 that interact with ACE2 and neutralizing antibodies. Cell Mol Immunol 2020;17(6):621–30.
[26] Procko E. The sequence of human ACE2 is suboptimal for binding the S spike protein of SARS coronavirus 2. bioRxiv. 2020.
[27] Krissinel E, Henrick K. Inference of macromolecular assemblies from crystalline state. J Mol Biol 2007;372(3):774–97.
[28] Kruger DM, Gohlke H. DrugScorePPI webserver: fast and accurate in silico alanine scanning for scoring protein-protein interactions. Nucleic Acids Res 2010;38(Web Server issue). W480-6.
[29] Humphrey W, Dalke A, Schulten K. VMD: Visual molecular dynamics. J Mol Graph 1996;14(1):33–8.
[30] Shah M, Anwar MA, Park S, Jafri SS, Choi S. In silico mechanistic analysis of IRF3 inactivation and high-risk HPV E6 species-dependent drug response. Sci Rep 2015;5:13446.
[31] Pearce R, Huang X, Setiawan D, Zhang Y. EvoDesign: designing protein-protein binding interactions using evolutionary interface profiles in conjunction with an optimized physical energy function. J Mol Biol 2019;431(13):2467–76.
[32] Upadhyaya P, Qian Z, Selner NG, Clippinger SR, Wu Z, Briesewitz R, et al. Inhibition of Ras signaling by blocking Ras-effector interactions with cyclic peptides. Angew Chem Int Ed Engl 2015;54(26):7602–6.
[33] Kaspar AA, Reichert JM. Future directions for peptide therapeutics development. Drug Discov Today 2013;18(17–18):807–17.
[34] Fosgerau K, Hoffmann T. Peptide therapeutics: current status and future directions. Drug Discov Today 2015;20(1):122–8.
[35] Achek A, Shah M, Seo JY, Kwon HK, Gui X, Shin HJ, et al. Linear and rationally designed stapled peptides abrogate TLR4 pathway and relieve inflammatory symptoms in rheumatoid arthritis rat model. J Med Chem 2019;62(14):6495–511.
[36] Lindorff-Larsen K, Piana S, Palmo K, Maragakis P, Klepeis JL, Dror RO, et al. Improved side-chain torsion potentials for the Amber ff99SB protein force field. Proteins 2010;78(8):1950–8.
[37] Pronk S, Páll S, Schulz R, Larsson P, Bjelkmar P, Apostolov R, et al. GROMACS 4.5: a high-throughput and highly parallel open source molecular simulation toolkit. Bioinformatics 2013;29(7):845–54.
[38] Wang H, Dommert F, Holm C. Optimizing working parameters of the smooth particle mesh Ewald algorithm in terms of accuracy and efficiency. J Chem Phys 2010;133(3):034117.
[39] Kumari R, Kumar R. Open source drug discovery C, Lynn A. g_mmpbsa–a GROMACS tool for high-throughput MM-PBSA calculations. J Chem Inf Model 2014;54(7):1951–62.
[40] Pettersen EF, Goddard TD, Huang CC, Couch GS, Greenblatt DM, Meng EC, et al. UCSF Chimera–a visualization system for exploratory research and analysis. J Comput Chem 2004;25(13):1605–12.
[41] Sukhwal A, Sowdhamini R. Oligomerisation status and evolutionary conservation of interfaces of protein structural domain superfamilies. Mol Biosyst 2013;9(7):1652–61.

[42] Anwar MA, Panneerselvam S, Shah M, Choi S. Insights into the species-specific TLR4 signaling mechanism in response to Rhodobacter sphaeroides lipid A detection. Sci Rep 2015;5:7657.
[43] Wolber G, Langer T. LigandScout: 3-D pharmacophores derived from protein-bound ligands and their use as virtual screening filters. J Chem Inf Model 2005;45(1):160–9.
[44] Mark James Abraham, Teemu Murtola, Roland Schulz, Szilárd Páll, Jeremy C. Smith, Berk Hess, et al. GROMACS: High performance molecular simulations through multi-level parallelism from laptops to supercomputers. SoftwareX. 2015;1–2:19-25.
[45] Crawford KHD, Eguia R, Dingens AS, Loes AN, Malone KD, Wolf CR, et al. Protocol and reagents for pseudotyping lentiviral particles with SARS-CoV-2 spike protein for neutralization assays. Viruses 2020;12(5).
[46] Adhikary P, Kandel S, Mamani UF, Mustafa B, Hao S, Qiu J, et al. Discovery of small anti-ACE2 peptides to inhibit SARS-CoV-2 infectivity. Adv Ther (Weinh) 2021;2100087.
[47] Pomplun S, Jbara M, Quartararo AJ, Zhang G, Brown JS, Lee YC, et al. De novo discovery of high-affinity peptide binders for the SARS-CoV-2 spike protein. ACS Cent Sci 2021;7(1):156–63.
[48] Norman A, Franck C, Christie M, Hawkins PME, Patel K, Ashhurst AS, et al. Discovery of cyclic peptide ligands to the SARS-CoV-2 spike protein using mRNA display. ACS Cent Sci 2021;7(6):1001–8.
[49] Karoyan P, Vieillard V, Gomez-Morales L, Odile E, Guihot A, Luyt CE, et al. Human ACE2 peptide-mimics block SARS-CoV-2 pulmonary cells infection. Commun Biol 2021;4(1):197.
[50] Pei P, Qin H, Chen J, Wang F, He C, He S, et al. Computational design of ultrashort peptide inhibitors of the receptor-binding domain of the SARS-CoV-2 S protein. Brief Bioinform 2021.
[51] Cao L, Goreshnik I, Coventry B, Case JB, Miller L, Kozodoy L, et al. De novo design of picomolar SARS-CoV-2 miniprotein inhibitors. Science 2020.
[52] Linsky TW, Vergara R, Codina N, Nelson JW, Walker MJ, Su W, et al. De novo design of potent and resilient hACE2 decoys to neutralize SARS-CoV-2. Science 2020.
[53] Planas D, Veyer D, Baidaliuk A, Staropoli I, Guivel-Benhassine F, Rajah MM, et al. Reduced sensitivity of SARS-CoV-2 variant Delta to antibody neutralization. Nature 2021.
[54] Gobeil SM, Janowska K, McDowell S, Mansouri K, Parks R, Stalls V, et al. Effect of natural mutations of SARS-CoV-2 on spike structure, conformation and antigenicity. bioRxiv 2021.
[55] Drescher DG, Ramakrishnan NA, Drescher MJ. Surface plasmon resonance (SPR) analysis of binding interactions of proteins in inner-ear sensory epithelia. Methods Mol Biol 2009;493:323–43.
[56] Yang D, Singh A, Wu H, Kroe-Barrett R. Comparison of biosensor platforms in the evaluation of high affinity antibody-antigen binding kinetics. Anal Biochem 2016;508:78–96.
[57] Schardt JS, Pornnoppadol G, Desai AA, Park KS, Zupancic JM, Makowski EK, et al. Discovery and characterization of high-affinity, potent SARS-CoV-2 neutralizing antibodies via single B cell screening. Sci Rep 2021;11(1):20738.
[58] Aparicio B, Casares N, Egea J, Ruiz M, Llopiz D, Maestro S, et al. Preclinical evaluation of a synthetic peptide vaccine against SARS-CoV-2 inducing multiepitopic and cross-reactive humoral neutralizing and cellular CD4 and CD8 responses. Emerg Microbes Infect 2021;10(1):1931–46.
[59] Schmidt F, Weisblum Y, Muecksch F, Hoffmann HH, Michailidis E, Lorenzi JCC, et al. Measuring SARS-CoV-2 neutralizing antibody activity using pseudotyped and chimeric viruses. J Exp Med 2020;217(11).
[60] Baisa G, Rancour D, Mansfield K, Burns M, Martin L, Cunha D, et al. A recombinant protein SARS-CoV-2 candidate vaccine elicits high-titer neutralizing antibodies in macaques. Res Sq 2021.
[61] Tan CW, Gardiner BS, Hirokawa Y, Smith DW, Burgess AW. Analysis of Wnt signaling beta-catenin spatial dynamics in HEK293T cells. BMC Syst Biol 2014;8:44.
[62] Zost SJ, Gilchuk P, Case JB, Binshtein E, Chen RE, Nkolola JP, et al. Potently neutralizing and protective human antibodies against SARS-CoV-2. Nature 2020;584(7821):443–9.
[63] Ju B, Zhang Q, Ge J, Wang R, Sun J, Ge X, et al. Human neutralizing antibodies elicited by SARS-CoV-2 infection. Nature 2020;584(7819):115–9.
[64] Cao Y, Su B, Guo X, Sun W, Deng Y, Bao L, et al. Potent neutralizing antibodies against SARS-CoV-2 identified by high-throughput single-cell sequencing of convalescent patients' B cells. Cell 2020;182(1):73–84 e16.
[65] Lefranc MP, Pommie C, Ruiz M, Giudicelli V, Foulquier E, Truong L, et al. IMGT unique numbering for immunoglobulin and T cell receptor variable domains and Ig superfamily V-like domains. Dev Comp Immunol 2003;27(1):55–77.
[66] Sievers F, Wilm A, Dineen D, Gibson TJ, Karplus K, Li W, et al. Fast, scalable generation of high-quality protein multiple sequence alignments using Clustal Omega. Mol Syst Biol 2011;7:539.
[67] Kemp SA, Collier DA, Datir R, Ferreira I, Gayed S, Jahun A, et al. Neutralising antibodies in Spike mediated SARS-CoV-2 adaptation. medRxiv 2020.
[68] Scheid JF, Barnes CO, Eraslan B, Hudak A, Keeffe JR, Cosimi LA, et al. B cell genomics behind cross-neutralization of SARS-CoV-2 variants and SARS-CoV. Cell 2021;184(12):3205–21 e24.
[69] Huo J, Zhao Y, Ren J, Zhou D, Duyvesteyn HME, Ginn HM, et al. Neutralization of SARS-CoV-2 by destruction of the prefusion spike. Cell Host Microbe 2020;28(3):445–54 e6.
[70] Valiente PA, Wen H, Nim S, Lee J, Kim HJ, Kim J, et al. Computational design of potent D-peptide inhibitors of SARS-CoV-2. J Med Chem 2021;64(20):14955–67.
[71] Shang J, Wan Y, Luo C, Ye G, Geng Q, Auerbach A, et al. Cell entry mechanisms of SARS-CoV-2. Proc Natl Acad Sci U S A 2020;117(21):11727–34.
[72] Andre Watson, Leonardo Ferreira, Peter Hwang, Jinbo Xu, Stroud R. Peptide Antidotes to SARS-CoV-2 (COVID-19). biorxiv. 2020.
[73] Tada T, Fan C, Chen JS, Kaur R, Stapleford KA, Gristick H, et al. An ACE2 microbody containing a single immunoglobulin Fc domain is a potent inhibitor of SARS-CoV-2. Cell Rep 2020;33(12):108528.
[74] Monteil V, Kwon H, Prado P, Hagelkruys A, Wimmer RA, Stahl M, et al. Inhibition of SARS-CoV-2 infections in engineered human tissues using clinical-grade soluble human ACE2. Cell 2020;181(4):905–13 e7.
[75] Polack FP, Thomas SJ, Kitchin N, Absalon J, Gurtman A, Lockhart S, et al. Safety and efficacy of the BNT162b2 mRNA covid-19 vaccine. N Engl J Med 2020.
[76] Walsh EE, Frenck Jr RW, Falsey AR, Kitchin N, Absalon J, Gurtman A, et al. Safety and immunogenicity of two RNA-based covid-19 vaccine candidates. N Engl J Med 2020;383(25):2439–50.
[77] Sacco MD, Ma C, Lagarias P, Gao A, Townsend JA, Meng X, et al. Structure and inhibition of the SARS-CoV-2 main protease reveal strategy for developing dual inhibitors against M(pro) and cathepsin L. Sci Adv 2020;6(50).
[78] Panda PK, Arul MN, Patel P, Verma SK, Luo W, Rubahn HG, et al. Structure-based drug designing and immunoinformatics approach for SARS-CoV-2. Sci Adv 2020;6(28). eabb8097.
[79] Xia S, Liu M, Wang C, Xu W, Lan Q, Feng S, et al. Inhibition of SARS-CoV-2 (previously 2019-nCoV) infection by a highly potent pan-coronavirus fusion inhibitor targeting its spike protein that harbors a high capacity to mediate membrane fusion. Cell Res 2020;30(4):343–55.
[80] Hopkins AL, Groom CR. The druggable genome. Nat Rev Drug Discov 2002;1(9):727–30.
[81] Schutz D, Ruiz-Blanco YB, Munch J, Kirchhoff F, Sanchez-Garcia E, Muller JA. Peptide and peptide-based inhibitors of SARS-CoV-2 entry. Adv Drug Deliv Rev 2020;167:47–65.
[82] Zhao H, To KKW, Lam H, Zhou X, Chan JF, Peng Z, et al. Cross-linking peptide and repurposed drugs inhibit both entry pathways of SARS-CoV-2. Nat Commun 2021;12(1):1517.
[83] Chorev M, Roubini E, McKee RL, Gibbons SW, Goldman ME, Caulfield MP, et al. Cyclic parathyroid hormone related protein antagonists: lysine 13 to aspartic acid 17 [i to (i + 4)] side chain to side chain lactamization. Biochemistry 1991;30(24):5968–74.
[84] Harrison RS, Shepherd NE, Hoang HN, Ruiz-Gomez G, Hill TA, Driver RW, et al. Downsizing human, bacterial, and viral proteins to short water-stable alpha helices that maintain biological potency. Proc Natl Acad Sci U S A 2010;107(26):11686–91.
[85] Curreli F, Victor SMB, Ahmed S, Drelich A, Tong X, Tseng CK, et al. Stapled peptides based on human angiotensin-converting enzyme 2 (ACE2) potently inhibit SARS-CoV-2 infection in vitro. mBio 2020;11(6).
[86] Li Y, Zheng X, Tang L, Xu W, Gong M. GLP-1 analogs containing disulfide bond exhibited prolonged half-life in vivo than GLP-1. Peptides 2011;32(6):1303–12.
[87] Castelletto V, Hamley IW, Seitsonen J, Ruokolainen J, Harris G, Bellmann-Sickert K, et al. Conformation and aggregation of selectively PEGylated and lipidated gastric peptide hormone human PYY3-36. Biomacromolecules 2018;19(11):4320–32.